

AD-A048 899

AIR FORCE INST OF TECH WRIGHT-PATTERSON AFB OHIO SCH--ETC F/G 20/11
NONLINEAR COLLAPSE ANALYSIS OF CYLINDRICAL SHELLS.(U)
DEC 77 N L COMPTON

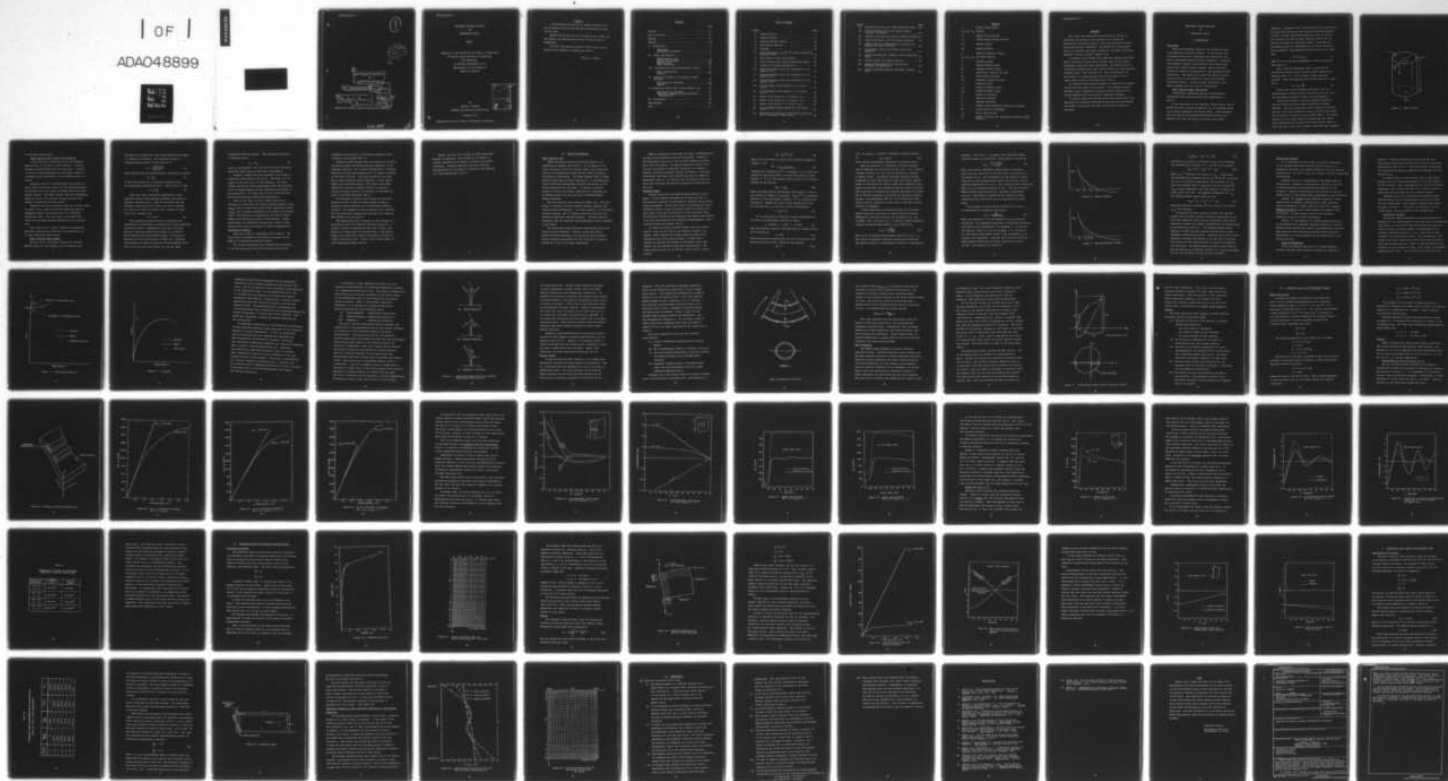
UNCLASSIFIED

AFIT/GA/AA/77D-2

NL

| OF |

ADA048899



END

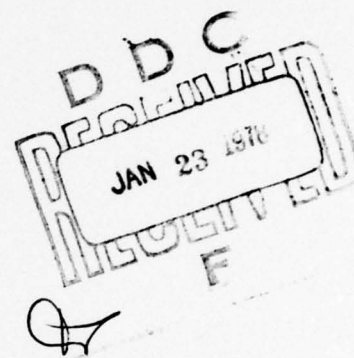
DATE

FILMED

2 - 78

DDC

①



⑥

NONLINEAR COLLAPSE ANALYSIS
OF
CYLINDRICAL SHELLS.

⑭

AFIT/GA/AA/77D-2

⑩

Norton L. ^{Leslie} Compton

⑨

Master's Thesis
+

⑪ Dec 77

⑫ 82p.

Approved for public release; distribution unlimited

012 225

y/B

NONLINEAR COLLAPSE ANALYSIS
OF
CYLINDRICAL SHELLS

THESIS

Presented to the Faculty of the School of Engineering
of the Air Force Institute of Technology
Air University
in Partial Fulfillment of the
Requirements for the Degree of
Master of Science

by
Norton L. Compton
Graduate Astronautical Engineering

December 1977

Approved for public release; distribution unlimited.

ACCESSION #	
NTIS	File Section <input checked="" type="checkbox"/>
DDC	Buff Section <input type="checkbox"/>
UNANNOUNCED	<input type="checkbox"/>
SECTION	
DISTRIBUTION/AVAILABILITY CODES	
SPECIAL	
A	

Preface

I am extremely grateful to Dr. Anthony Palazotto for his invaluable guidance and unfailing willingness to help at all times.

Special thanks also go out to Katheryn Lore Riddle for her support and understanding during the final weeks of preparation.

I am also very deeply indebted to Mary Turner for her patience and diligence in typing this thesis.

Norton L. Compton

Contents

	Page
Preface.	ii
List of Figures.	iv
Symbols.	vi
Abstract	vii
I. Introduction	1
Background	1
Preliminary Statement.	6
II. Theory and Modeling	9
STAGS Computer Code.	9
Instability Concepts	16
Brazier Effect	23
White Besseling.	26
III. Stiffened Shells with Rectangular Cutouts.	30
Model Descriptions	30
Results.	31
IV. Plasticity Analysis of an Axially Loaded Cylinder.	48
Description of the Model	48
Results.	51
V. Cylindrical Shell Under a Pure Bending Load.	59
Description of the Model	59
Additional Comments on Ring Stiffener Configuration.	63
VI. Conclusions	66
Bibliography	69
Vita	71

List of Figures

Figure	Page
1. Shell Geometry.	3
2. Newton's Method14
3. Modified Newton's Method.14
4. Bifurcation Buckling.18
5. Collapse.19
6. Load Displacement Curves for Various Bifurcation Buckling Cases.22
7. Ovalization of the Cross Section.25
8. Stress Strain Curve Showing Baushinger Effect .	.28
9. Internal Stiffener Configuration.32
10. Load Displacement Curve for Stiffened 12 x 12 Cutout; $t=0.1$33
11. Load Displacement Curve for Stiffened 24 x 24 Cutout; $t=0.1$34
12. Load Displacement Curve for Stiffened 24 x 24 Cutout; $t=0.2$35
13. W Displacement Field Around 24 x 24 Cutout; $t=0.1$37
14. W Displacement Field Around 12 x 12 Cutout; $t=0.1$38
15. Moment Field Around 24 x 24 Cutout; $t=0.1$39
16. Moment Field Around 12 x 12 Cutout; $t=0.1$40
17. Moment Field Around 6 x 6 Cutout; $t=0.1$42
18. W Displacement Fields Around 24 x 24 Cutout; $t=0.2$44
19. Comparison of Nonlinear Displacement Fields for 24 x 24 Cutouts at Common Load.45

Figure		Page
20.	Stress-Strain Curve for 304SS Stainless Steel .	.49
21.	Finite Difference Mesh for Axially Loaded Cylinder- No Cutout50
22.	Boundary Conditions for Axially Loaded Cylinders.	52
23.	Load Displacement Curve for Plastic Analysis. .	.54
24.	Stress Field in Circumferential Direction for Plastic and Linear Analysis55
25.	Displacement Curves for Plastic and Linear Analysis.57
26.	Linear and Nonlinear (Plastic) Stress Resultant Field58
27.	Analytic Model for Bending Analysis62
28.	Warping Plane Profiles for Various Ring Stiffener Configurations.64
29.	Finite Difference Mesh for End Moment Loading Case.65

Symbols

δ	lateral displacement
$e_x, e_\theta, e_{x\theta}$	strains
E	modulus of elasticity
D	strain energy density function
E_s	secant modulus
E_t	tangent modulus
F	vector of external forces
$\kappa_x, \kappa_\theta, \kappa_{x\theta}$	curvature changes
L	cylinder length
M	applied bending moment
\bar{M}	collapse bending moment
N	amplitude of applied end load
N_x	axial stress resultant
η_s	plasticity reduction factor
ν	Poisson's ratio
ν_E	elastic Poisson's ratio
ν_p	plastic Poisson's ratio
ρ	radius of curvature
r	radius of cylinder
t	cylinder thickness
$\bar{\sigma}$	maximum axial compressive stress at collapse
Δw	cross sectional flattening
u	total strain energy
z^i	vector of strains and rotational changes at mesh station i

ABSTRACT

This study was carried out to determine the effects of plasticity and cutouts on the buckling of stiffened and nonstiffened cylindrical shells. Axial and end moment loading configurations were considered. The problem was investigated using the nonlinear and linear branches of the STAGS (Structural Analysis of General Shells) computer code.

It becomes clear through this study that cutouts positioned within cylindrical shells create results that are not easily predictable using past shell experiences. The moment field in a nonlinear analysis has a much greater effect on a more flexible structure than a less flexible one. This characteristic is not present in a linear analysis due to the removal of the higher order rotation terms that effect strain.

An elastic/plastic analysis appears to precipitate collapse in much the same manner as do cutouts. The collapse results obtained using a completely nonlinear plastic analysis can be closely approximated using Gerard's plasticity equation.

To prevent warping of the end plane under bending two rings separated by a distance determined by the parallel axis theorem are needed to counteract the lack of rotational rigidity in the shell.

NONLINEAR COLLAPSE ANALYSIS

OF

CYLINDRICAL SHELLS

I. Introduction

Background

Within the Aerospace industry, the cylindrical shell is an important structural element. In the earlier days of powered flight shell structures were typified by thin skins strengthened through internal stiffening. Technological advances, however, have dictated that aircraft and missile skins become thicker, thereby, making plasticity effects an important consideration in the problem of shell instability. This thesis will study the effects of plasticity as well as the effects of cutouts on stiffened cylindrical shells. A ring-stiffened cylindrical shell under a bending load will also be investigated.

Shell Buckling Under Compression

A preliminary background sketch of the history of cylindrical shell buckling under axial compression is useful.

In the early part of the twentieth century Lorenz (Ref 1) became the first to write an equation for the buckling stress in an axially compressed cylindrical shell. Lorenz assumed that the buckling and prebuckling deformations were axisymmetric and that the edges of the shell were simply

supported. Timoshenko (Ref 2) improved upon the inaccuracies in Lorenz work and derived the classical buckling equation in 1910. In 1911 Lorenz also became the first to publish work relating the case of axial buckling without the restriction of symmetric deformation modes. He assumed in his analysis that the displacements in an axial direction were negligible. The boundary conditions used in his study were

$$v^* = w^* = M_x = 0 \quad (1)$$

where v^* and w^* are the displacements v and w at buckling (See Figure 1).

Next, Seide and Weingarten (Ref 3) predicted the bifurcation buckling load by using a linear membrane pre-buckling state for a finite length, simply supported cylinder. These researchers found the maximum axial stress to be

$$\bar{\sigma} = 0.6 \frac{Et}{r} \quad (2)$$

Three years later Timoshenko determined that the nonaxisymmetric buckling stress was identical to the classical axisymmetric buckling stress given by Equation 2.

There were, however, two basic problems associated with the buckling patterns hereto predicted by linear theories. The first being that axially symmetric buckling can only occur when plasticity occurs, violating the assumption of perfect elasticity in the linear theory. The second problem was that linear theory predicted that the entire shell surface would be covered with small buckles where in fact only one or two rows of buckles occur with the remainder

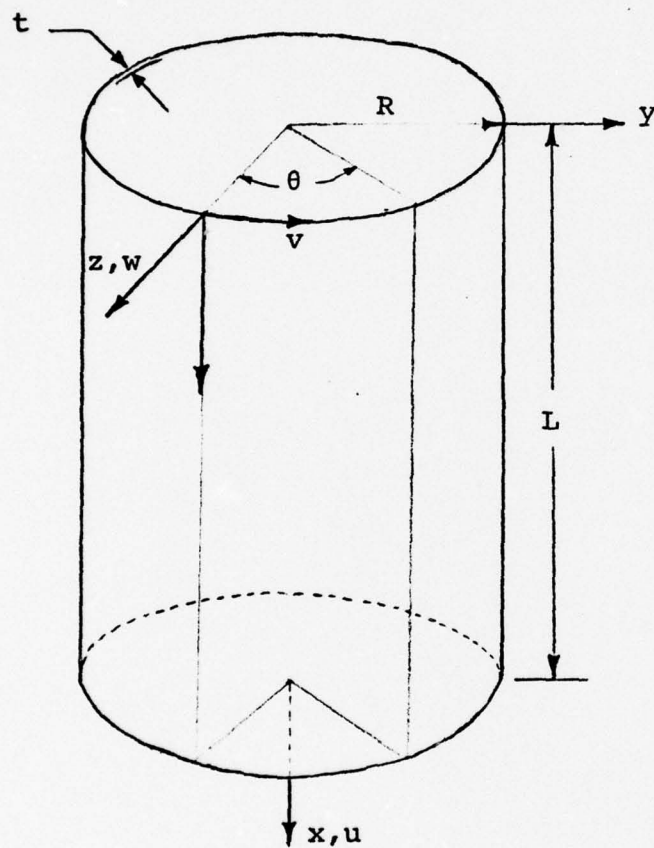


Figure 1. Shell Geometry

of the shell being smooth.

Shell Buckling with Cutouts and Stiffeners

In the design of cylindrical shells for aerospace applications, it has been a common practice to impose boundary discontinuities upon the shell skin. Internal or external shell stiffening has also become common to strengthen areas susceptible to local buckling due to a cutout.

Palazotto (Ref 4) has investigated the validity of using linear bifurcation theory for the buckling analysis of stringer and ring-stringer stiffened shells with rectangular cutouts. The STAGS computer code was incorporated using the linear and nonlinear collapse analyses with smeared and discrete stiffener theory.

Palazotto was able to conclude that for a narrow region of cutout sizes, linear bifurcation theory was able to adequately predict the buckling load of a stiffened cylindrical shell. This was based on the result that linear and nonlinear analyses differed by only a few per cent.

This thesis will, in part, attempt to substantiate the above conclusion and determine its applicability to a larger variety of cutout sizes.

Shell Buckling Under Bending

Brazier (Ref 5) was able to predict the critical bending moment for the collapse of an infinitely long

cylinder by minimizing the total strain energy with respect to a change in curvature. The resulting critical or collapse bending moment, \bar{M} , was found to be

$$M = \frac{2(2)^{\frac{1}{2}} E \pi r t}{9(1-\nu^2)^{\frac{1}{2}}} \quad (3)$$

which occurred when the cross-sectional flattening Δw reached

$$\Delta w = \frac{2}{9} r \quad (4)$$

If the axial stress due to bending is computed using the undistorted cross-section with ν taken to be 0.3, then

$$\sigma = 0.33 \frac{Et}{r} \quad (5)$$

Aksel'rad (Ref6) reported an improvement of this buckling study by simultaneously including the effects of geometric nonlinearities. Aksel'rad contended that the collapse stress varied from $0.6Et/r$ for short cylinders to a value of $0.3Et/r$ for shells with a length to radius ratio, (L/r) , greater than

$$2.5 (r/t)^{\frac{1}{2}} \quad (6)$$

Much research has been devoted to analytical and experimental investigations of buckling of axially compressed cylindrical shells. Considerable less effort has been devoted to the more complicated problem of cylindrical shell buckling under pure bending loads. The paucity of knowledge in this area has made it common for engineers and designers to relate the critical maximum bending stress (σ_b) to the critical axial stress (σ_c) for the axial

compression buckling problem. This procedure translates in equation form as

$$\sigma_b = C\sigma_c \quad (7)$$

where σ_c is presumed to be known and C has been previously determined from testing or empirical relationships.

Recently, emphasis has been centered on the study of relatively thick shells, such as $R/t < 50$, where R is the radius of the shell and t is the thickness. For these thicker shells very little experimental data was available, so it had become common for some researchers to estimate C by extrapolation (or direct use) of the C value for thin shells which had been studied more extensively.

Prior to the 1960's it was a common practice for designers to assume that the critical maximum bending stress ($\sigma_{b_{max}}$) was 1.3 times the critical axial compressive stress ($\sigma_{c_{max}}$) for a cylinder regardless of the radius to thickness ratio. This practice was supported by the lack of experimental and theoretical results to the contrary. Recent experimental and theoretical results have, however, shed serious doubt about the validity of such an approximation.

Preliminary Statement

Three main areas are researched in this thesis. The first being an analysis of the effects of cutouts on the behavior of stiffened cylindrical shells.

The critical parameters that a designer must consider or at least appreciate when he is involved with the def-

formation, stress field, or instability problem of shell structures is addressed (Ref 7).

Within the past fifteen years the problem of stiffened cylindrical shells has become genuinely important to the aerospace industry. As a further consideration, a designer would like to know the characteristics of symmetric cutouts on the shell structure. The major question is how does one go about analyzing these structures? linear theory? Hooke's Law? nonlinear theory? This thesis uses STAGS (Structural Analysis of General Shells) to consider a variety of typical shells in an attempt to shed some new light on the above questions (Ref 8).

Of particular interest in this study was the determination of when cutouts are large enough to require nonlinear elastic equations for a sufficiently accurate solution. For purposes of such an analysis four cylinders with discontinuities imposed upon the shell were analyzed both linearly and nonlinearly.

The second main area of endeavor is the analysis of a cylindrical shell with inelastic material properties. A relative paucity of research has been done in this area, making it a prime target for investigation. More specifically, this thesis will address the plastic collapse of a thick cylindrical shell, $r/t=50$, that is quite common in civil engineering fields (Ref 9).

Lastly, the case of a cylindrical shell under pure bending is addressed. This problem is of concern to nuclear engineers in the design of reactor and related facilities. Boundary conditions and end stiffening configurations are discussed in relation to the modeling of a pure bending load (Ref 10).

II. Theory and Modeling

STAGS Computer Code

STAGS (Structural Analysis of General Shells) is a comprehensive computer code (Ref11). It is capable of the static analysis of shells of general shape, and includes the effects of nonlinearities caused by both material behavior and geometric deformation. The STAGS computer code is fundamentally based upon an energy formulation. A two-dimensional finite difference approximation replaces derivatives in the energy expressions for the shell. To obtain a solution, energy is forced to be stable, resulting in a nonlinear set of equations which are then solved by a modified Newton-Raphson technique.

Two main branches exist within the STAGS code. The first branch is limited to strictly elastic material behavior and contains three sub-branches: (1) linear analysis, (2) nonlinear collapse analysis, and (3) buckling analysis based upon the classical bifurcation buckling approach. Collapse loads are determined when the nonlinear load-displacement curve approaches a limit point.

The second main branch contained within STAGS allows for plastic material behavior. However, unlike the elastic branch discussed previously, the plasticity section allows neither temperature gradients nor the variation of material properties in any of the space coordinates.

STAGS is applicable to any shell for which a mathematically suitable finite difference grid can be defined. Generally, the investigator uses one of the ten shell geometry routines built into the program. If another shape were desired, then the user may provide a subprogram describing the geometry. Cutouts, discrete stiffeners, smeared stiffeners, a multitude of boundary conditions, and virtually any type of loading is permissible (Ref 11). In addition, for the elastic branch the shell wall thickness and material properties through the wall may vary.

Solution Method

A brief overview of the STAGS solution method is given below. A more detailed treatment can be found in (Ref 7). The numerical solution is predicated on rendering the potential energy stationary. This is done with a two-dimensional finite difference scheme in which the shell surface is covered with grid (mesh) lines that run parallel to the coordinate lines. The degrees of freedom of the system are the normal displacements, w , at the grid points and the tangential displacements, u and v , centered between grid points (Fig 1).

To obtain the total potential energy, the total strain energy, U and the work done by the external forces W , are needed. STAGS computes the strain energy by numerically integrating the strain energy density. To make such a integration possible the surface of the shell is into sub-regions that are defined by mesh line intersections. The strain energy density at an arbitrary mesh station i can be written

$$\Delta U^i = \frac{1}{2} Z^{iT} D^i Z^i \quad (8)$$

where Z^i is the vector of strains and curvature changes at station i , and

$$Z^{iT} = \{e_x e_\theta e_{x\theta} k_x k_\theta k_{x\theta}\} \quad (9)$$

indicates the transpose of Z^i . In general, Z^i is a nonlinear function of the displacement and their derivatives at mesh station i . D^i is a 6x6 positive definite matrix of constants defined by the relation

$$D_{kl}^i = \Delta U_{,kl}^i \quad (10)$$

where the comma denotes differentiation with respect to one of the strains or changes in curvature. Since Z^i is a quadratic function of the displacement unknowns, ΔU^i is a fourth order polynomial. Summing the strain energy contributions from all the subareas, a_i , the total strain energy becomes

$$U = \sum_i \Delta U^i a^i \quad (11)$$

If F is the vector of external forces corresponding to the vector of displacement unknowns X , where,

$$X = \{u_v^1 w^1 \text{ --- } u_v^i w^i \text{ --- } u_v^n w^n\} \quad (12)$$

then the potential energy of the work done by external forces can be written as

$$W = X^T F \quad (13)$$

Static equilibrium requires that the first variation of the potential energy be zero, leading to the equation

$$LX = F \quad (14)$$

L is, in general, a nonlinear "stiffness" operator defined

by
$$LX = \text{grad } U \quad (15)$$

which relates displacement components to external forces.

When the operator L is nonlinear, iterative methods must be employed for the solution of Eq. (14). For a general collapse analysis, Eq. (14) must be solved for a sequence of applied loads. A practical nonlinear analysis dictates a sequence of load steps, chosen so that the initial approximation of the solution is nearly linear and subsequent steps change the solution only moderately from one step to the next. This procedure is necessary for reliable detection of collapse due to the non-uniqueness of solutions to nonlinear equation systems. The requirement that $LX = F$ be solved many times using iterative procedures is what makes a nonlinear collapse analysis so expensive.

A brief description of Newton's method and the Newton-Raphson method for the case of a single variable function demonstrates the method used for the solution of Eq. (14) in STAGS. For a function $g(x) = 0$, Newton's method determines a better and better approximation, X_{i+1} , defined by

$$X_{i+1} = - \frac{g(X_i)}{g'(X_i)} \quad (16)$$

where X_i is the previous approximate solution to $g(X) = 0$.

The iterative procedure converges quadratically (provided the initial estimate is sufficiently accurate) to any desired

accuracy. (See Fig 2). In Figure 3 the "modified" Newton iteration scheme is illustrated. This method is defined by

$$X_{n+1} = \frac{X_n - g(X_n)}{g'(X_0)} \quad (17)$$

Thus, this method corresponds geometrically to extending lines from the curve $g(X)$ to the axis which are parallel to the tangent at X_0 . The convergence of this method is slower than that of the standard Newton method but does not require repeated computations of $g'(X)$. This is particularly significant when $g'(X)$ is extremely difficult to get. The most effective STAGS strategy usually calls for a periodic recomputation of $g'(X)$. Both Newton's method and the "modified" Newton method have been generalized to an n -dimensional Euclidean space.

For treatment of the nonlinear solution of Eq (14) it is advantageous to introduce the notation

$$L'_{ij} = \frac{\partial^2 U}{\partial X(i) \partial X(j)} \quad (18)$$

where the derivative L' of the operator L is an $n \times n$ matrix so defined. The elementary properties of ordinary derivations also hold for the derivations L' of operator L . As long as the nonlinear terms of L are not dropped, L' is a function of a particular displacement vector X and is denoted L'_X to indicate this dependence. With the use of Eq (18) above the Newton-Raphson method can be easily generalized to solve Eq (14). The iteration is defined by

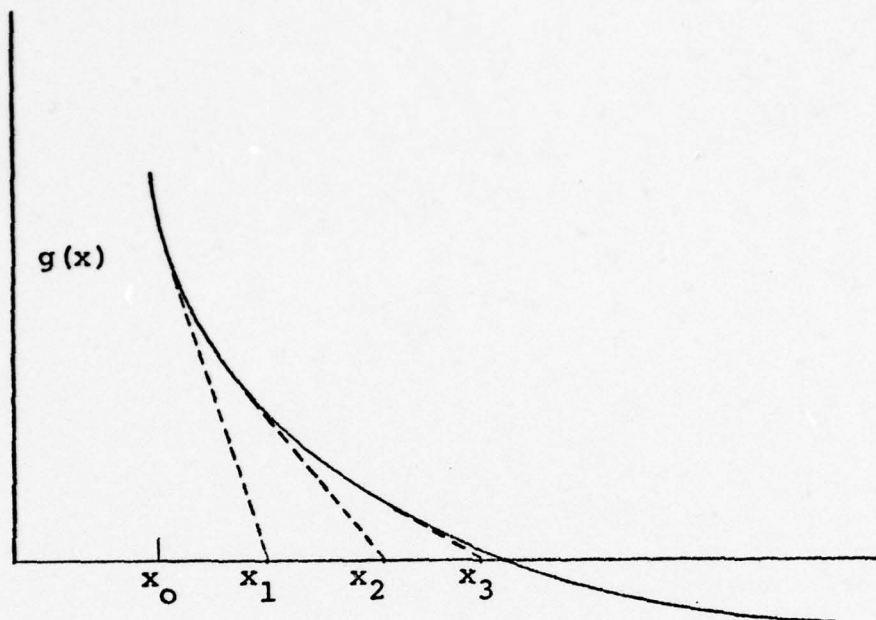


Figure 2. Newton's Method

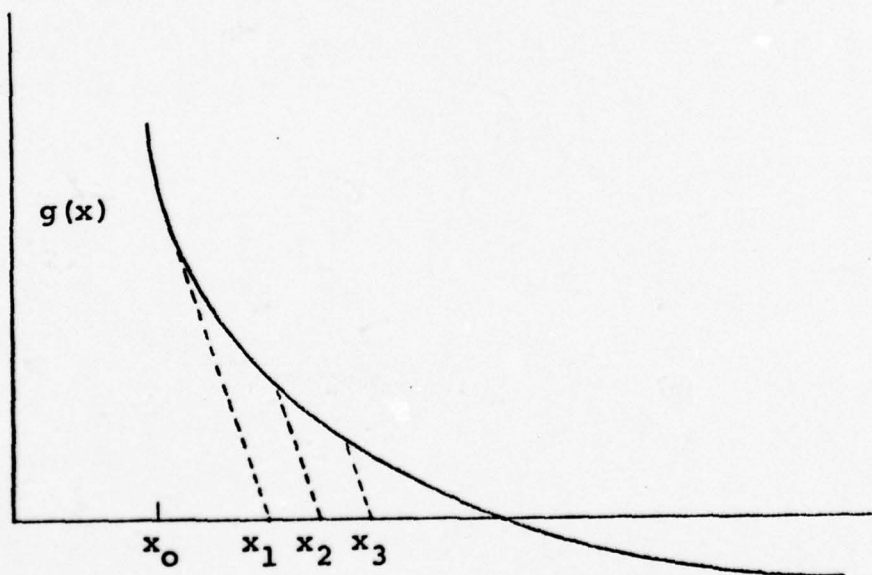


Figure 3. Modified Newton's Method

$$L'_{X_k} (X_{k+1} - X_k) = F - LX_k \quad (19)$$

Provided X_0 is close to a solution and L'_{X_k} is not singular, the iteration will converge to X . Eq (19) can be written

$$X_{k+1} = X_k + L'_{X_k}^{-1} (F - LX_k) \quad (20)$$

where $L'_{X_k}^{-1}$ indicates the inverse of L'_{X_k} . Reiterating, the most effective strategy for the use of Eq (20) in solving Eq (14) is a periodic recomputation and inversion of L'_{X_k} , since the computer time is required to do the inversion of L'_{X_k} is great compared to the time required to compute the other terms in Eq (20). For periodic computation of L'_{X_k} the modified Newton method takes the form

$$X_{k+1} = X_k + L'_{X_m}^{-1} (F - LX_k) \quad (21)$$

where the subscript m denotes the last iteration for which $L'_{X_m}^{-1}$ was computed.

In contrast to other iterative schemes, the modified Newton method provides accurate solutions independent of the load step (numerical error does not accumulate) while simultaneously avoiding the frequent recomputation and factorization of the derivative matrix L' . The modified Newton method employed in STAGS provides rigorous results with the most economical computational effort. Effective use of this method requires reasonably good choices as to the size of the load steps and as to when the derivative L' should be recomputed and refactored. The STAGS program contains as much built-in decision making as is feasible, however, it is still necessary for the user to choose the best overall "strategy".

Instability Concepts

It is worthwhile at this point to present a discussion of the concepts associated with the plastic behavior in instability problems, the possible effects of initial material imperfections, and some of the basic concepts of shell instability and buckling.

Collapse occurs as a combination of two basic types of nonlinearity. Geometric nonlinearities, usually in the form of rotations, effect the equilibrium formulations for the structure. Material nonlinearities are realized in the nonlinear nature of the stress-strain relationship of the structure.

Clearly, for linear elastic behavior collapse is attributed solely to geometric nonlinearities. More generally, plastic deformation of shell structures made from a strain-hardening material involve both material and geometric nonlinearities. In this general case the two nonlinear phenomenon interact to cause instability.

However, in the analysis of a strain hardened structure it is mandatory that geometric nonlinear effects be included. Omitting these effects will cause a load-displacement relationship where the load continually increases with increasing displacement at a rate controlled by the stress-strain curve of that material.

Types of Instability

A loss of stability may occur in a strain hardening structure through either geometric collapse or bifurcation

buckling. Bifurcation buckling results from the load-displacement curve being intersected by another equilibrium configuration (See Fig 4). The load obtained at the point of intersection is commonly termed the bifurcation load and designated P_b .

It must be kept in mind, however, that a bifurcation analysis is only a rough approximation to the real behavior of the structure. When nonlinearities are large, bifurcation techniques lose accuracy and thus are no longer valuable in predicting buckling loads at small computer expense.

Collapse occurs in an intrinsically different manner than bifurcation and is represented as the point at which the load displacement curve reaches a maximum (zero slope) as shown in Figure 5 . This point is referred to as the "limit point", and P_c is known as the collapse load.

Bifurcation Buckling

Bifurcation buckling problems are characterized by the existence of two infinitesimally close equilibrium configurations. From Figure 4 it is evident that the primary path emanating from the origin (initially stable) is intersected by the secondary equilibrium path at $P = P_b$. This point is also referred to as the branching point. The equilibrium on the primary path can be shown to be stable below the bifurcation point and unstable above it. Thus, at the bifurcation point stability of the structure is lost. As a result, two possible phenomenon will occur. The structure will deform into the

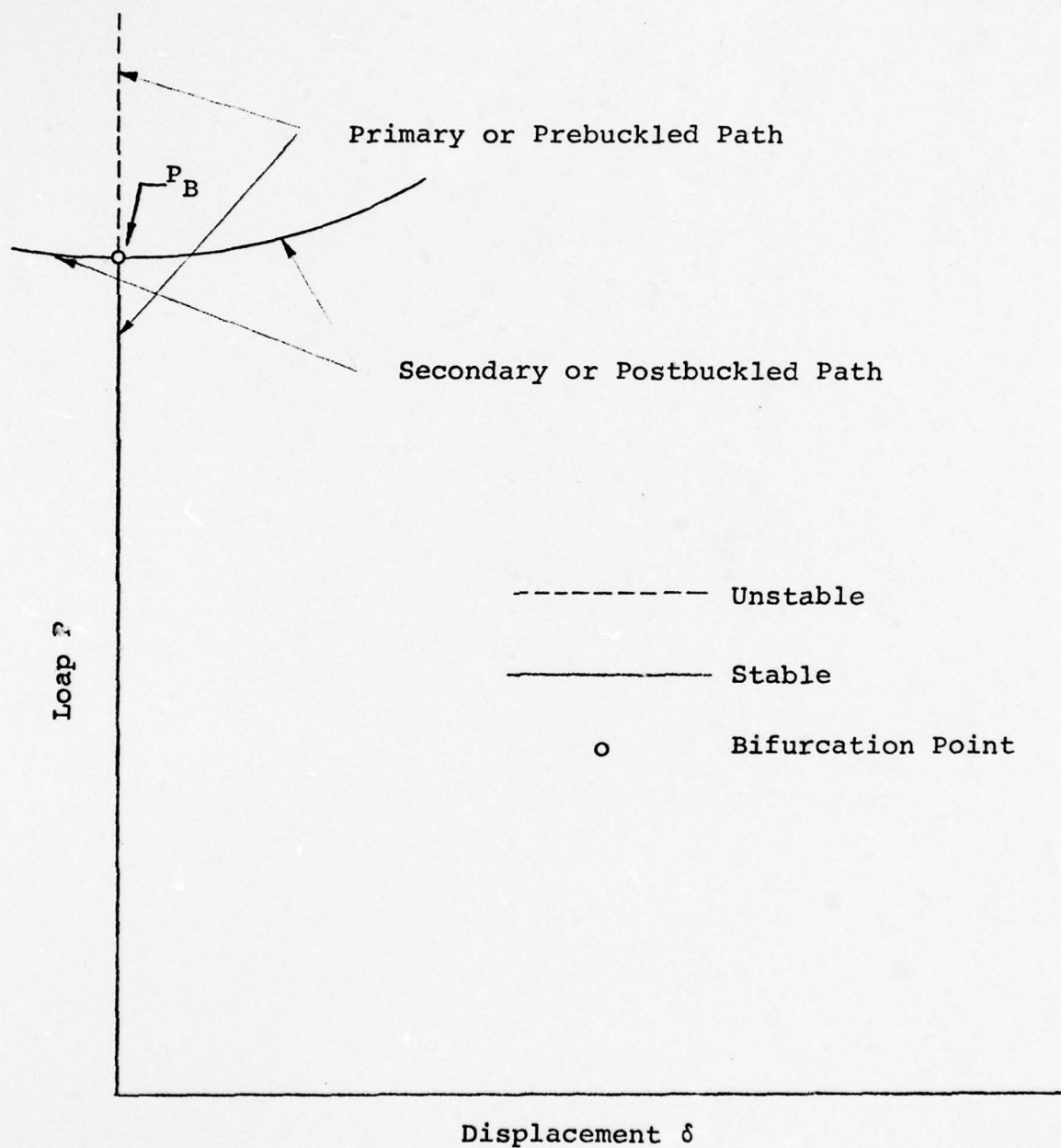


Figure 4. Bifurcation Buckling

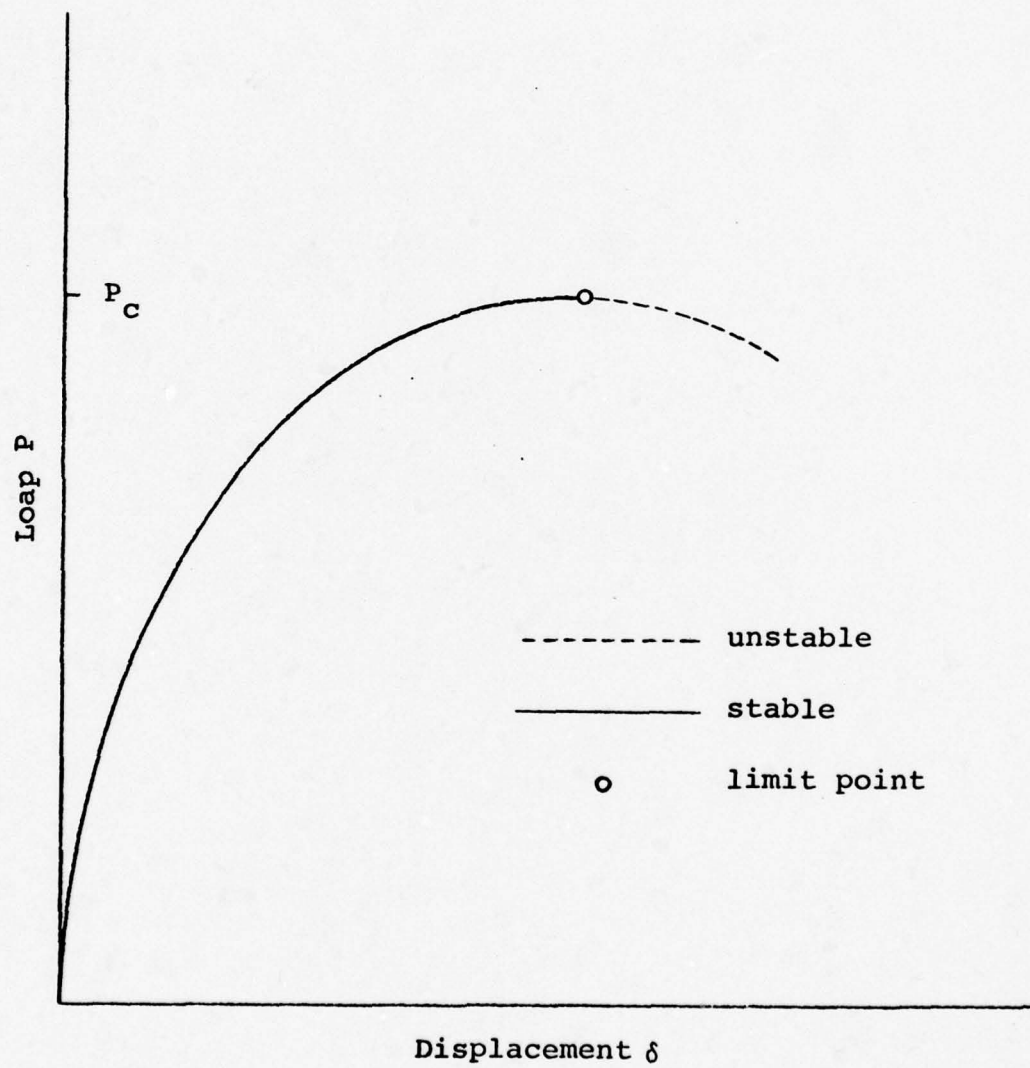


Figure 5. Collapse

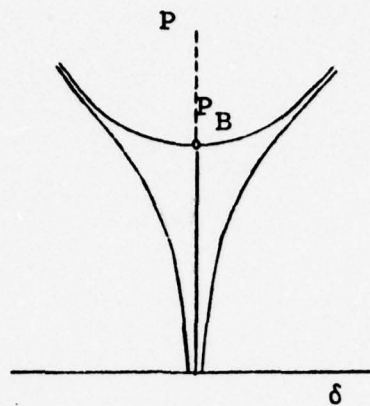
equilibrium configuration represented by the postbuckled (secondary) path or dynamic movement of the structure will occur. One of the above will occur depending on the stability of the postbuckling path. If the postbuckling path rises, it is stable and the structure will deform into another equilibrium configuration. Alternatively, a falling (stable) postbuckling path will cause the structure to be set into unstable motion. The postbuckling path is represented on a load-displacement curve in which the load P is plotted against the lateral displacement δ at some point in the structure. Each point then represents a possible equilibrium configuration for a given load.

An important consideration in the instability of structures is that bifurcation buckling cannot take place if the structure contains an initial imperfection. If such an imperfection exists the primary path only asymptotically approaches the path corresponding to the perfect structure. Structures are classified as imperfection sensitive or insensitive depending upon a rising or falling postbuckling path. Structures are classified as imperfection-sensitive when a relatively small imperfection leads to a drastic reduction in the load carrying ability of the structure. This case is characterized by a falling (unstable) postbuckling path. Stability loss of a structure that is imperfection-sensitive is due to collapse at the limit point on the load-displacement curve rather than through bifurcation.

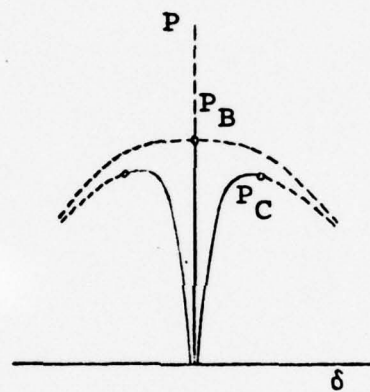
To reiterate, a real (imperfect) structure may lose stability either gradually or explosively depending on whether it is imperfection sensitive or not. The extent of imperfection sensitivity can be directly correlated to the initial shape of the postbuckling path of the corresponding bifurcating perfect structure. Based on this readily observable phenomenon, it is desirable to categorize bifurcation buckling problems into three different cases:

- (I) Stable-Symmetric (Imperfection-Insensitive)
- (II) Unstable-Symmetric (Imperfection-Sensitive)
- (III) Asymmetric (Imperfection-Sensitive)

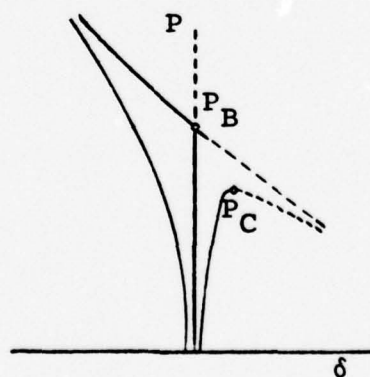
For Case I (Fig 6a) bifurcation buckling problems, the initial part of the postbuckling path for the perfect structure is rising, due to the stiffening effects of geometric nonlinearities. The equilibrium path for the imperfect structure approaches this postbuckling path with the deflections merely growing more rapidly as the buckling load of the structure is approached. Thus, for a purely elastic analysis the structure would not fail whereas for plastic behavior there is a continual decrease in the slope of the load displacement curve until a limit point is reached and collapse occurs. Where plasticity is introduced failure occurs at a deflection, δ that is, in general, large in comparison to the value of δ where the P - δ curve first departs from linearity. Regardless of plastic behavior it follows from the above that Case I structures are not sensitive to initial imperfections. As should be, there is only small scatter in test results



(a) Stable-Symmetric



(b) Unstable-Symmetric



(c) Asymmetric (Unstable)

Figure 6. Load Displacement Curves for Various Bifurcation Buckling Cases

for these structures. Besides simply supported cylinders in axial compression, columns, plates, and rings under uniform pressure are also imperfection insensitive. For imperfection-sensitive structures that exhibit either elastic or plastic behavior, the symmetric postbuckling path (Fig 6b) is falling (unstable). This is due to the softening nature of the geometric nonlinear effects. Explosive displacement will occur for such a structure at the limit point in the $P-\delta$ curve when a steadily increasing load is applied. It is intuitively satisfying that test results are of a widely scattered nature. Deep laterally loaded arches and shallow spherical caps under external pressure are highly imperfection sensitive.

Asymmetric imperfection-sensitive structures exhibit sensitivity with respect to positive imperfections, but not negative ones (Fig 6c). However, in a pragmatic sense it cannot be assumed that the structure has a tendency to favor one type of imperfection over the other. Hence, such structures are termed imperfection-sensitive (Ref 12).

Brazier Effect

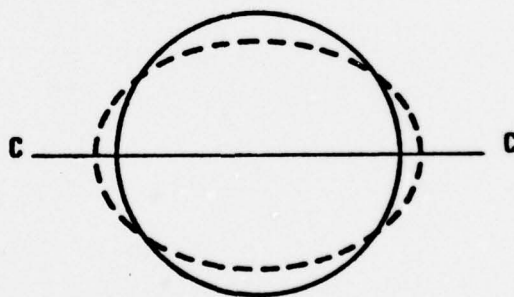
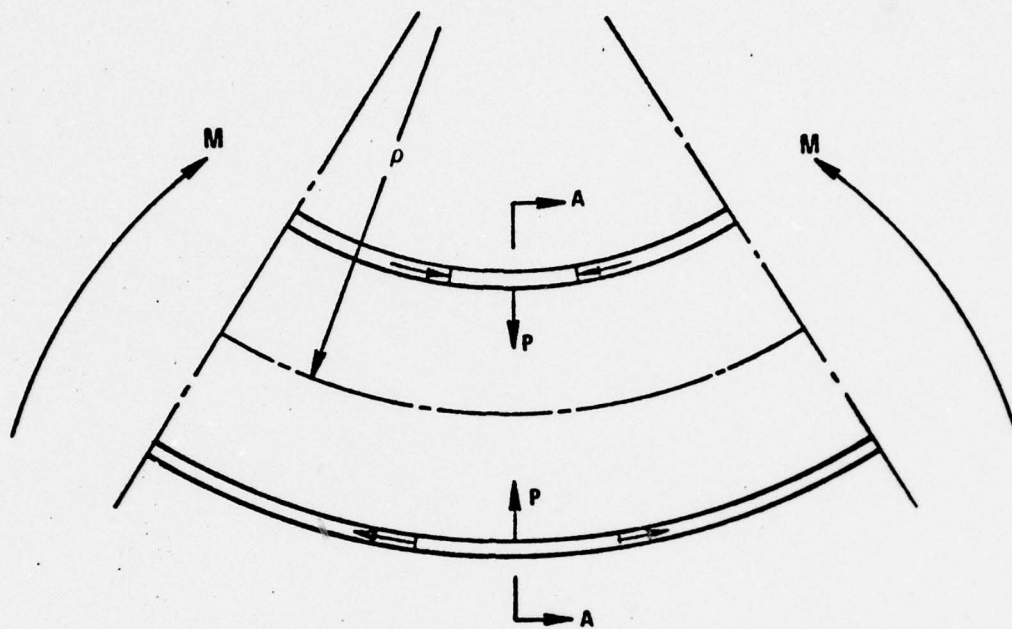
In many cylindrical shell analyses, it is assumed that prebuckling rotations are small enough to be neglected. This is a reasonably accurate assumption as long as the shell is sufficiently short. For long cylinders, or even medium length cylinders in which the end cross sections are not held circular, nonlinear prebuckling effects must not be

neglected. The most significant nonlinear prebuckling effect is the flattening (ovalization) of the cylinder cross section. This prebuckling deformation is commonly referred to as the Brazier effect. Due to the applied bending moment an axial curvature, $\kappa=1/\rho$, is induced. The resulting curvature causes the axial stress in an arbitrary fiber to have a component p directed towards the neutral axis of bending. Figure 7 shows the two extreme fibers (maximum tension and compression), and the corresponding components p . It is the net effect of these inward force components that cause the shell to deform into the oval shape indicated by the dotted line in Figure 7.

Four main consequences stem from the flattened cross section:

- (1) A fairly substantial redistribution of stress occurs.
- (2) The circumferential radius of curvature increases.
- (3) The cross section experiences a continual decrease in bending stiffness as the bending moment increases.
- (4) Nonlinear collapse occurs at a bending moment lower than the one predicted from the linear membrane prebuckled state.

Collapse due to the Brazier effect is actually collapse into a circumferential flattening mode. Determination of



SECTION A - A

Figure 7 Ovalization of the Cross Section

the collapse moment M_{Brazier} is obtained by plotting the variation of M with cross sectional flattening Δw . The reduction of bending stiffness with increasing moment results in the continual decrease in the slope of the M versus Δw curve. The slope will continue to decrease until a maximum value of M is reached at which time the slope will be zero. In equation form this can be written:

$$M_{\text{Brazier}} = (M) \frac{dM}{d\Delta w} = 0$$

Very long cylinders that are sufficiently thin will buckle in the Brazier mode due to the cross-sectional flattening discussed above. Alternately, short cylinders buckle into a many bifurcation mode characterized by small axial wrinkles or wavelengths. Shells between these two extremes demonstrate a coupling between the cross-sectional flattening and axial wrinkling modes.

White Besseling

The STAGS program implements the White Besseling plasticity theory. The White Besseling theory assumes that the shell material consists of several components which have identical elastic properties and exhibit ideal plasticity (no strain hardening), but have unequal yield strengths. Since the strain is identical in all components, the stress-strain curve will be marked by a decrease in slope as a stress approaches the yield point for any given component. When this point is reached the components will cease to take

any additional load. Thus, the "composite" exhibits strain hardening with a stress-strain curve that is piecewise linear. If the composite was comprised of only one component, ideal plasticity theory would be applicable.

If the loading (stress) is reversed after yield limit has been reached for one or more of the components, yield will occur in the opposite direction at a stress in the composite which is lower than that for original yield. (See Figure 8). Diagrammatically, tension is applied, OAB, beyond the yield limit which is followed by a strain reversal, BCD, into the compression yield zone (Figure 8). The yield ellipse for the weakest component is also shown in the figure. Note that yield in compression will occur when the total strain is $\epsilon_1 - 2\epsilon_y$. Thus, yield in compression will occur at a significantly lower stress if a prior tension overload has occurred. This phenomenon is known as the Bauschinger effect.

The Bauschinger effect involves two main factors. One is the nonuniformity of yielding in a polycrystalline metal. Because the crystals are oriented at random throughout the metal, they yield by different amounts so that on a microscopic scale the stress varies slightly from crystal to crystal. When the member is unloaded, it contracts until the average stress is zero, but the crystals that yielded the least do not quite return to zero and thus remain in tension, while those that yielded the most go beyond zero

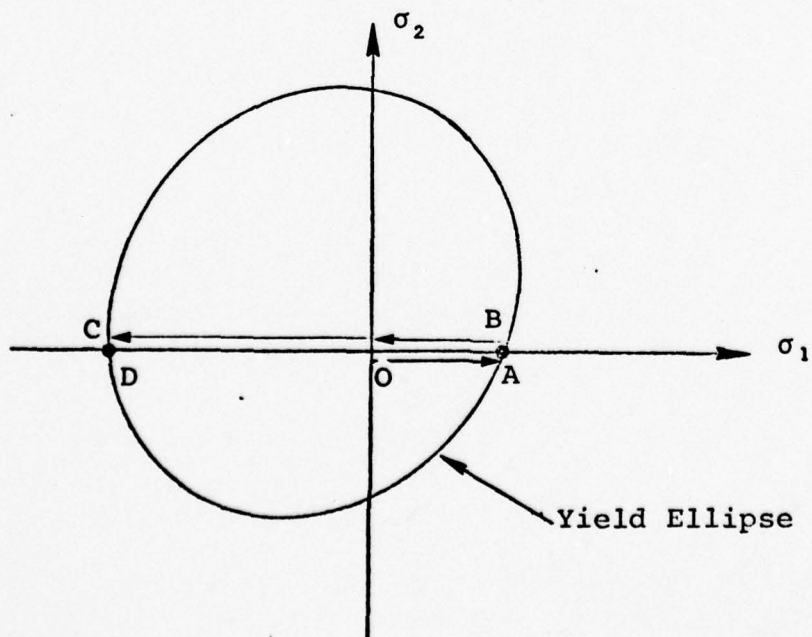
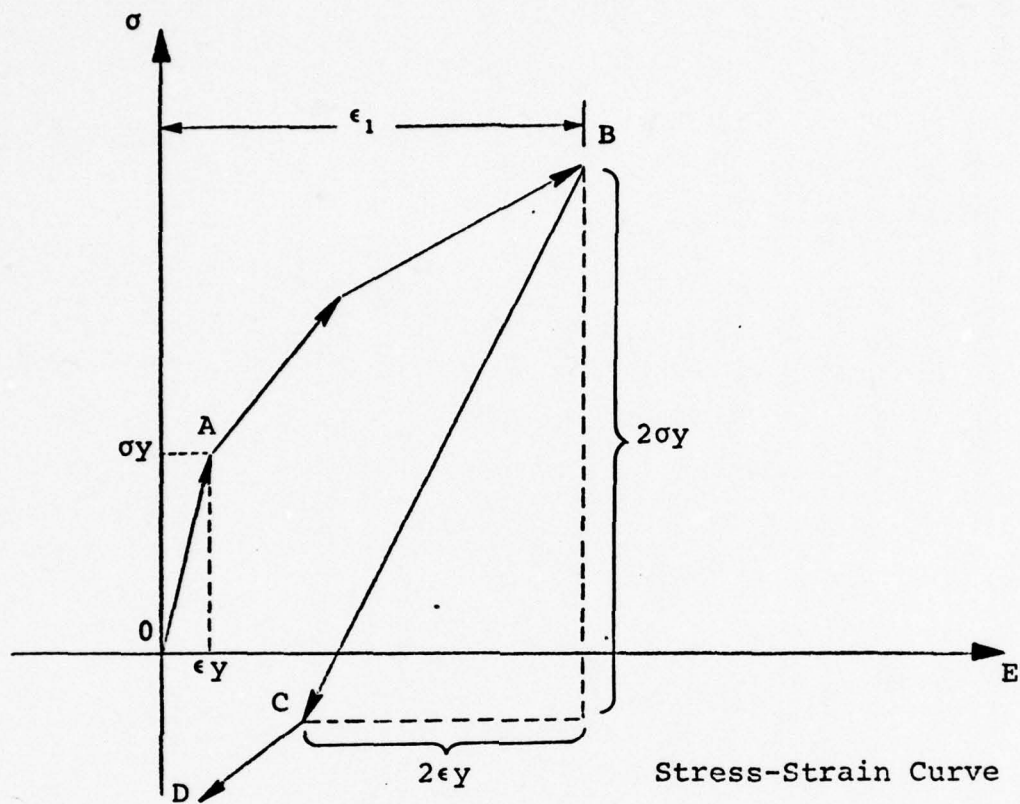


Figure 8 . Stress-Strain Curve Showing Bausinger Effect

and are under compression. Thus, there are microscopic residual stresses throughout the metal, some tension and others compression. When the material is then compressed after having been elongated, the crystals that have compressive residual stresses will yield at a lower-than-normal stress, and therefore the overall yield stress is lowered.

The White Besseling theory employed in STAGS simulates plasticity effects as described below:

- (1) The plastic behavior of the material is defined through specification of
 - the total number of components
 - the relative volume of each component
 - the yield strength of each component
- (2) The strains are estimated for all points by extrapolation from the previous solution.
- (3) For each of the material components the stress corresponding to the assumed strains is determined via a subroutine called from within. The total stress for the entire "composite" is then found.
- (4) With the total stresses and strains known, the inelastic part of the strain increment is determined and then added as a pseudo-load.
- (5) New strains are now re-extrapolated and used as new estimates. This procedure continues until sufficient agreement between estimated and computed strains is reached.

III. Stiffened Shells with Rectangular Cutouts

Model Descriptions

To study the effects of cutouts on stiffened shells, three sizes of boundary discontinuities were researched. Cutout dimensions were 6" x 6", 12" x 12", and 24" x 24", with shell thicknesses being 0.1". As a further consideration a shell containing a 24" x 24" cutout with a thickness of 0.2" was studied to provide information on thickness effects. To best approximate a typical aerospace structure the following shell parameters were used:

$$\frac{L}{r} = 1.64$$

$$\frac{r}{t} = 57.3$$

The material properties of the shells are as follows:

$$E = 1.0 \times 10^7 \text{ psi}$$

$$\nu = 0.333$$

$$G = 3.75 \times 10^6 \text{ psi}$$

$$t = 0.1", 0.2"$$

The shells are internally stiffened in the axial direction by means of stringers placed a distance of three inches apart. The basic material properties

$$E = 1.0 \times 10^7 \text{ psi}$$

$$\nu = 0.333$$

remain the same as the shell itself. Each stringer possesses a cross-sectional area of 0.28 inches squared with moments of inertia:

$$I_y = 1.493 \times 10^{-2} \text{ in}^4$$

$$I_z = 2.8583 \times 10^{-3} \text{ in}^4$$

$$I_x = 3.0302 \times 10^{-4} \text{ in}^4$$

The stringers are 0.8 inches in height and have an eccentricity (distance from inner surface of shell to stiffener centroid in z' direction) of .4 inches. Figure 9 depicts the stiffener configuration.

Boundary conditions imposed upon the shells are shown in Figure 22. On boundary line 1, movement is allowed in the U direction only. The other three boundaries possess symmetry which implies that

$$u = \beta = 0 \quad \text{On line 3}$$

$$v = \beta = 0 \quad \text{On lines 2 and 4}$$

Results

Table I contains the critical and collapse loads based upon linear bifurcation and nonlinear STAGS computer runs. Figures 10, 11, and 12 represent the load displacement curves for the shells containing the 12 x 12, 24 x 24 ($t = .1$), and 24 x 24 ($t = .2$) cutouts respectively.

Cutouts: 24 x 24, 12 x 12, 6 x 6; $t = .1$

The most startling result observed is the apparent inconsistency between P_{cr} and P_{coll} as the cutout is enlarged. For the 24 x 24 cutout ($t = .1$) a knockdown of 5.92% occurs between linear and nonlinear analysis. Surprisingly, a larger knockdown of 14.39% occurs for the 12 x 12 cutout. Such an occurrence is far from being intuitively clear.

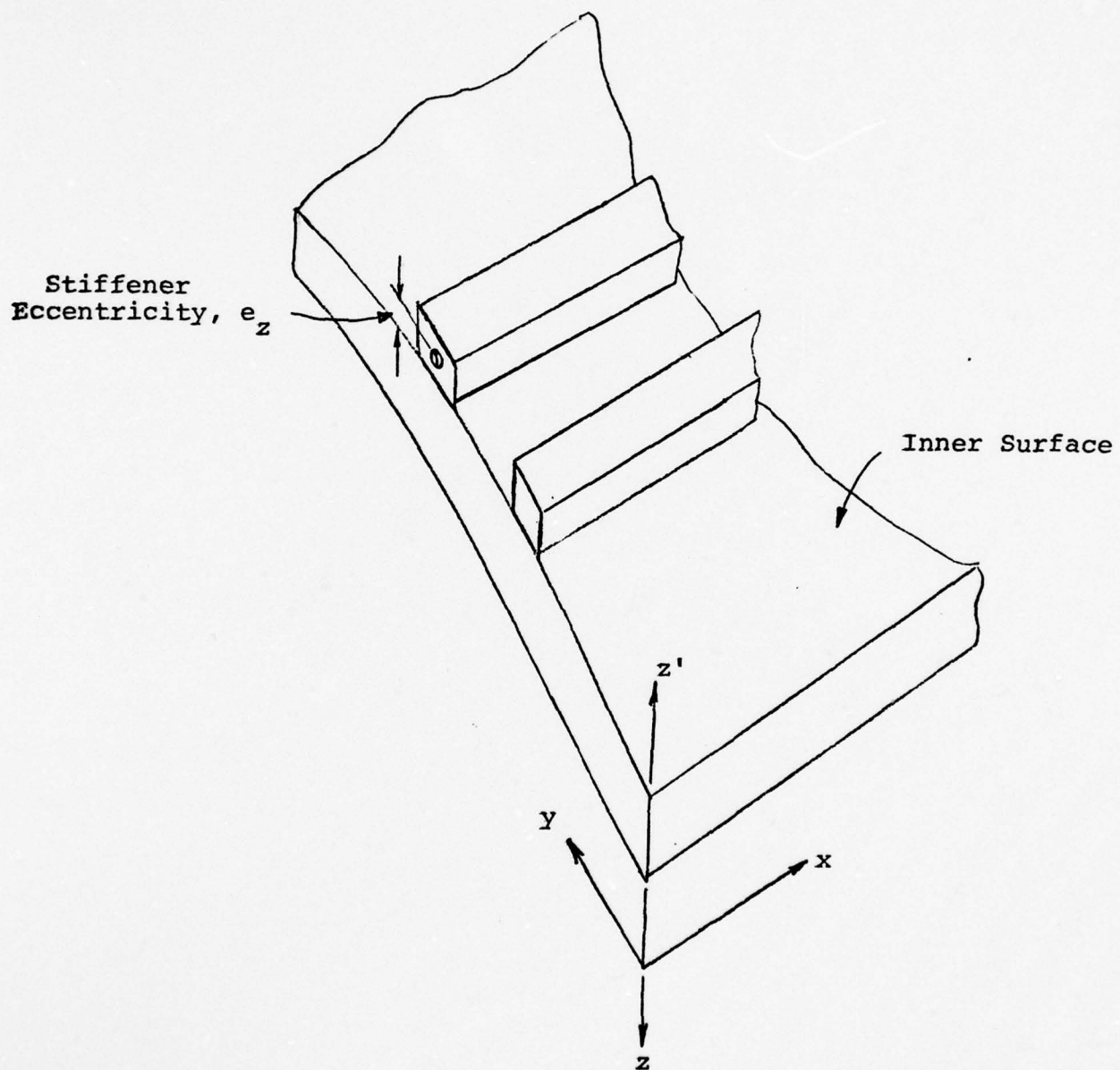


Figure 9. Internal Stiffener Configuration

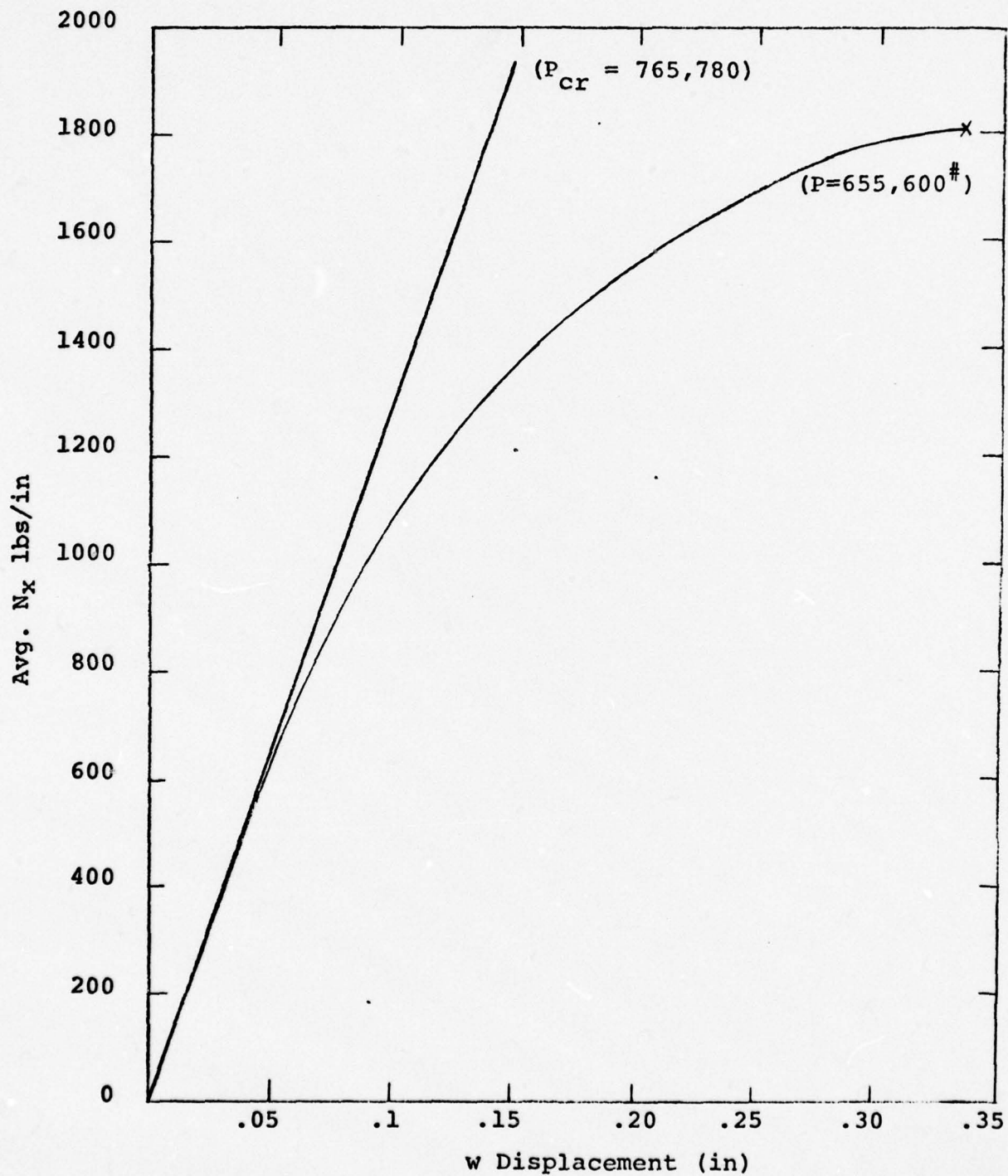


Figure 10. N_x vs w (stringer stiffened)
12" x 12" Cutout

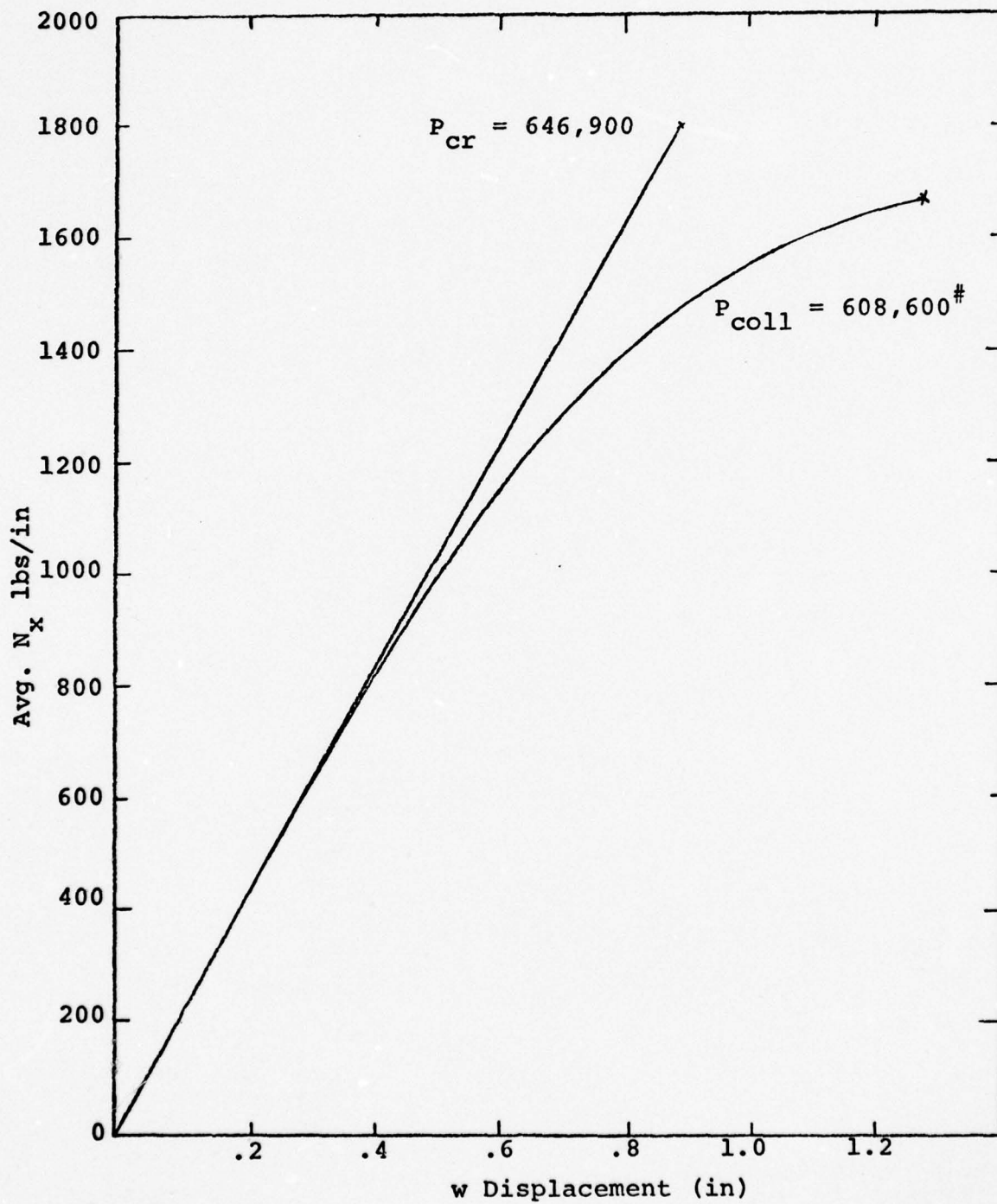


Figure 11. N_x vs w (stringer stiffened)
24" x 24" Cutout; $t = .1$

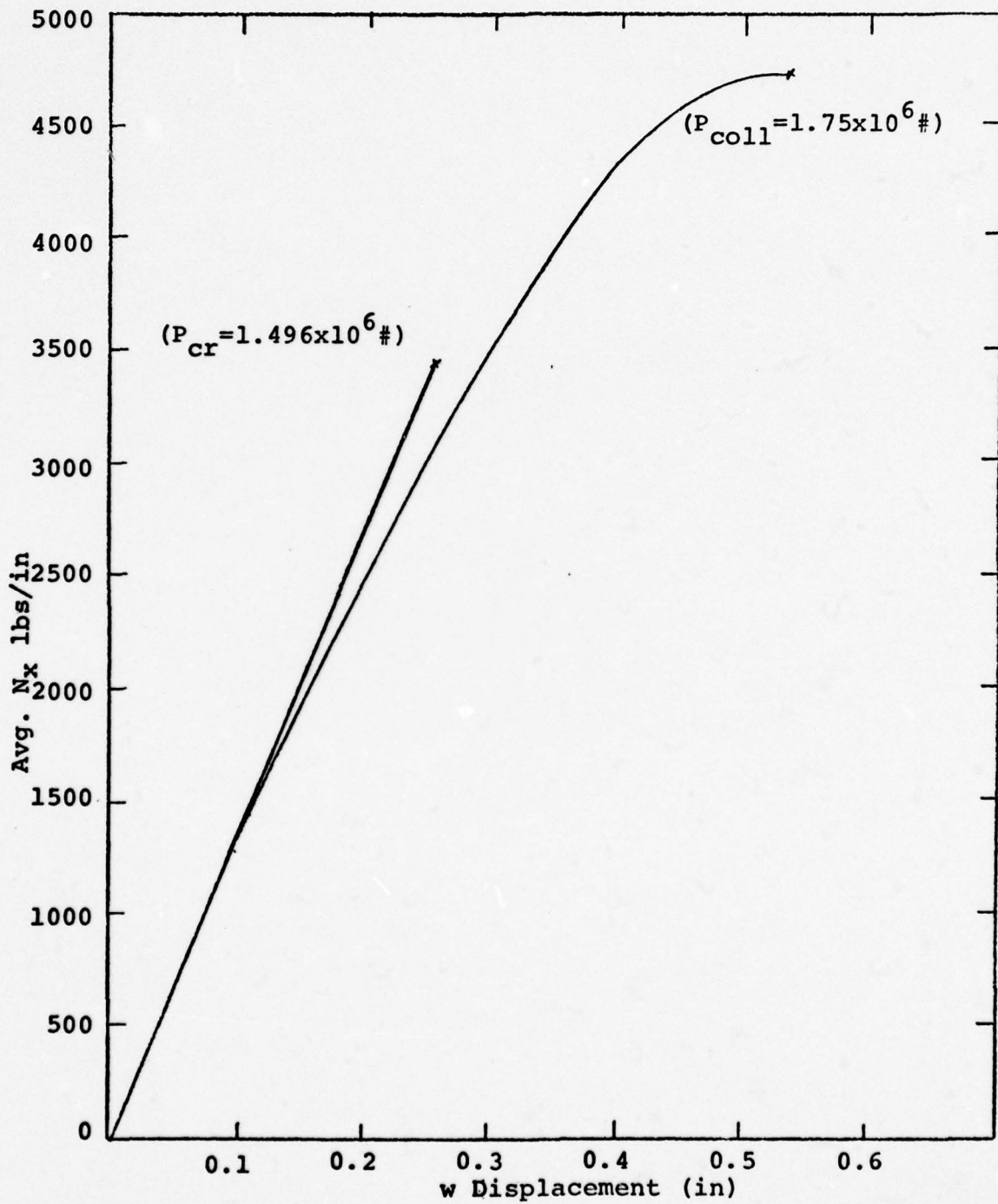


Figure 12. N_x vs w (stringer stiffened)
24" x 24" Cutout; $t = .2$

An explanation for the unexpected result that the 24 x 24 cutout produces a closer agreement between linear and nonlinear theories lies in the w displacement field around the cutout. For the 24 x 24 cutout it is evident from Figure 13 that the large w displacements are localized solely in the region of the cutout. However, as seen in Figure 14 the displacements field does not dissipate for the 12 x 12 cutout.

This is an important result, for only upon examination of the moment fields, in connection with the displacement field is it possible to understand the mechanisms involved in the unexpected linear/nonlinear relationship.

Examination of Figures 15 and 16 reveal very similar moment patterns. Moment distribution and magnitude are virtually identical in both axial and circumferential traverses. Thus, the concept emerges that similar moment fields applied to different displacement fields will result in dissimilar collapse characteristics.

The same moment field acting on two shells, will naturally precipitate collapse on the shell with greater displacements, for this shell has been more severely "weakened" by a greater warping of its surface.

In essence then, the shell containing the 24 x 24 cutout is stiffer than expected due to a noticeable lack of w displacements away from the cutout. It follows that linear and nonlinear theories should predict a closer buckling load for this structure.

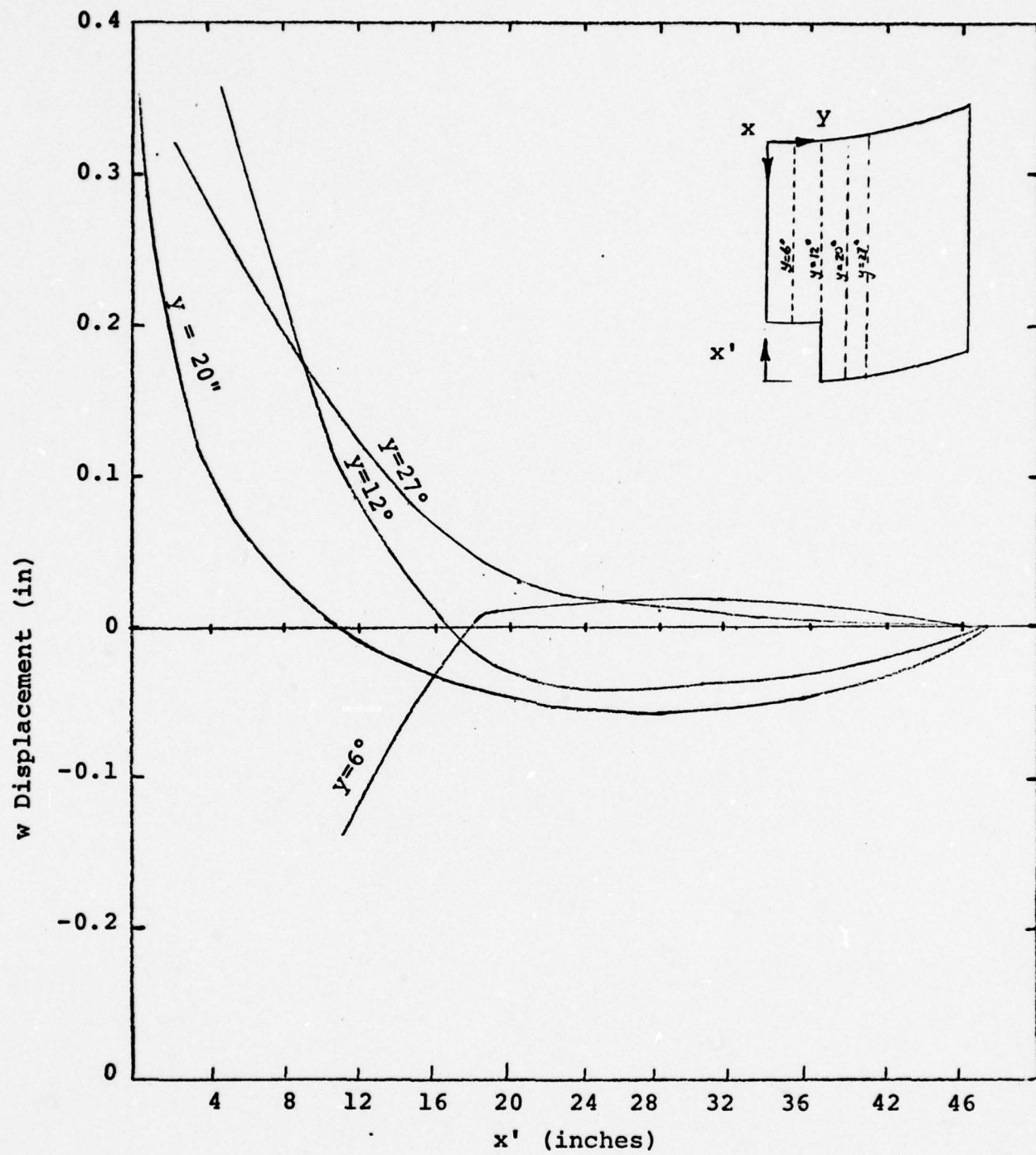


Figure 13. w Displacement Field Around
24" x 24" Cutout; $t = .1$

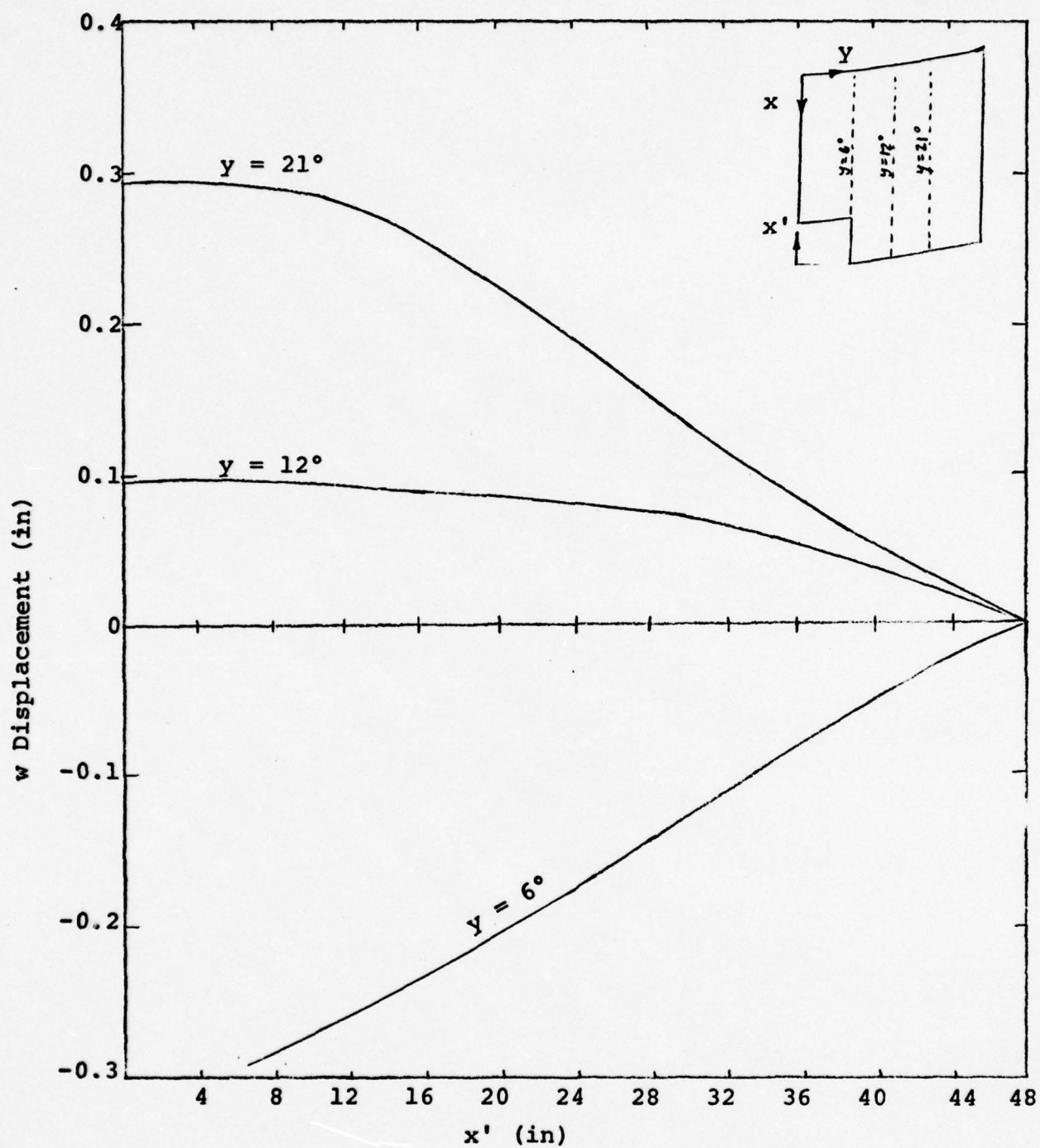


Figure 14. w Displacement Field Around
12" x 12" Cutout; $t = .1$

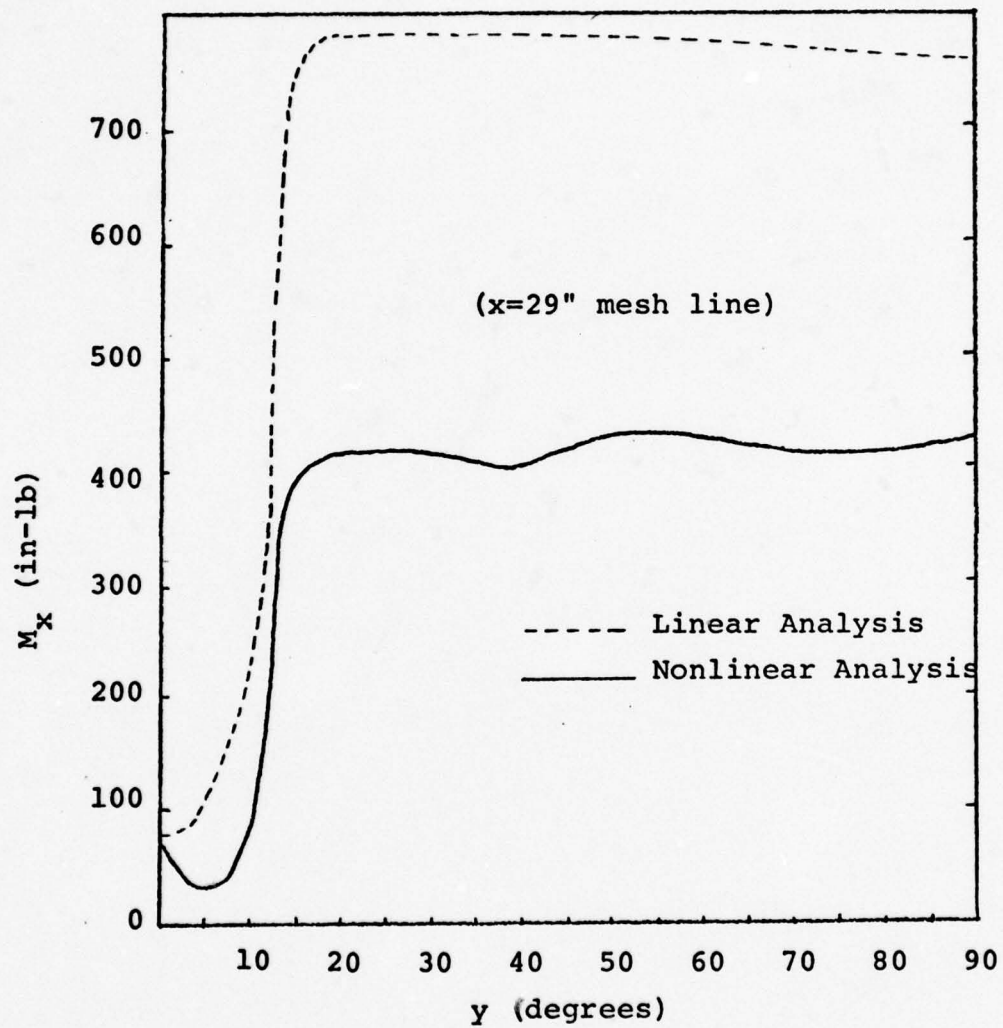


Figure 15. Moment Field Around
24" x 24" Cutout; $t = .1$

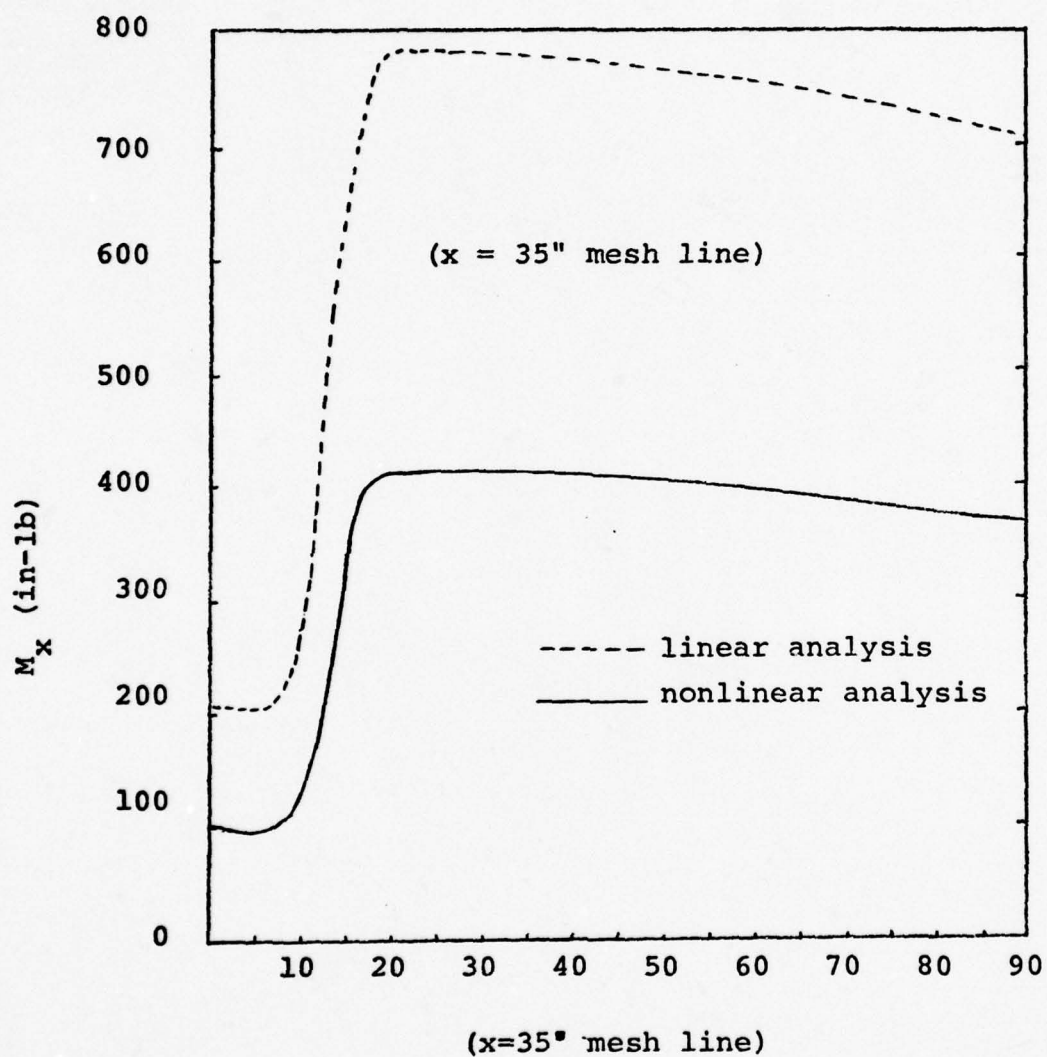


Figure 16. Moment Field Around
12" x 12" cutout; $t = .1$

In the case of the 12 x 12 cutout the w displacement field does not diminish away from the cutout. This allows the moment field to interact with the deleterious effects of the warping. The net result is a larger gap between linear and nonlinear theories.

To further investigate the cutout size effect on displacement and moment distribution a 6 x 6 cutout was investigated. A linear bifurcation study was made but circumstances precluded a nonlinear analysis.

Figure 17 illustrates a moment concentration very similar to that found in the analysis of the 24 x 24 cutout. Figure 18 reveals a displacement profile that is, like the 24 x 24 cutout, quite localized. It appears from this data that the 6 x 6 cutout reacts in a similar fashion to the 24 x 24 cutout. A rather good agreement between linear and nonlinear theories is expected based upon this similiarity. A nonlinear run should reveal a displacement pattern resembling that obtained for the linear run, and indicate a collapse load in good agreement with the linear predicted critical load.

Cutout 24 x 24; t = .2

Analysis of this cylinder also produced surprising results. Figure 12 reveals that the nonlinear collapse load was 14.3% higher than the critical load obtained from a bifurcation analysis. What has happened in this case is that the mechanisms that acted to cause a weaker shell nonlinearly for .1" shell have reversed their effect and

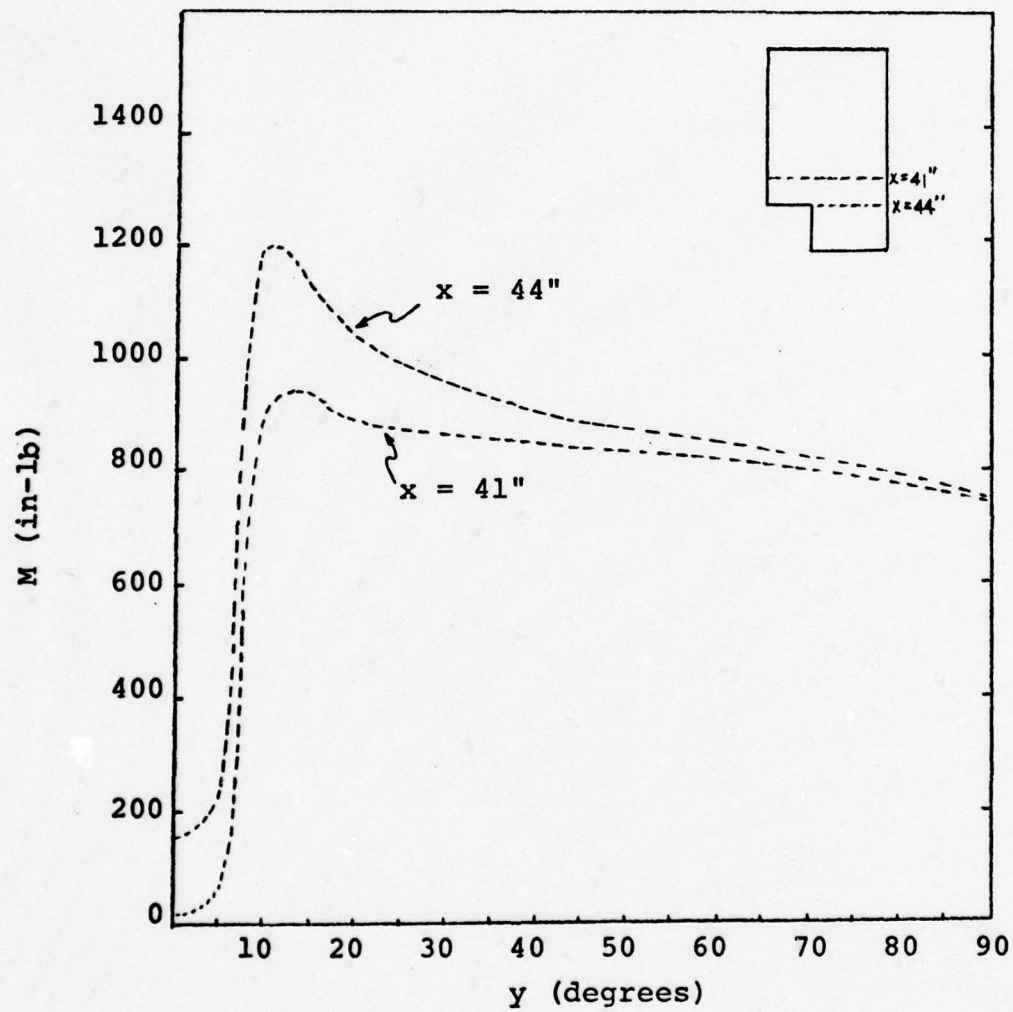


Figure 17. Moment Field Around
6" x 6" Cutout; $t = .1$

have caused a more flexible shell in the linear analysis. This implies that the displacement field is now larger for the linear analysis. Figure 18 documents this observation.

In the nonlinear analysis the moment-displacement interaction is being resisted by the increased thickness. The increase in thickness is responsible for a much smaller moment field around the cutout and a correspondingly greater load carrying capability. The linear case does not experience the increased thickness effects in the same way due to the omission of higher order rotation terms. Thus, it is the large variation in the nonlinear analysis that is responsible for the reversal.

It is instructive to examine the nonlinear displacement fields for both thicknesses at a common load level. By this means an approximation of their comparative stiffnesses can be made. Figure 19 demonstrates that the thicker shell is indeed stiffer and therefore should collapse at a higher load level. This result has also been documented.

Consequently, displacement fields have become the primary source of comparison in evaluating shell capabilities in resisting axial loads.

In previous paragraphs we have displayed a reasoning behind the variation between linear and nonlinear analyses for a variety of cutout sizes.

It is observable from Table I that the collapse results for the 12 x 12 cutout and the $t=0.1$, 24 x 24 cutout were

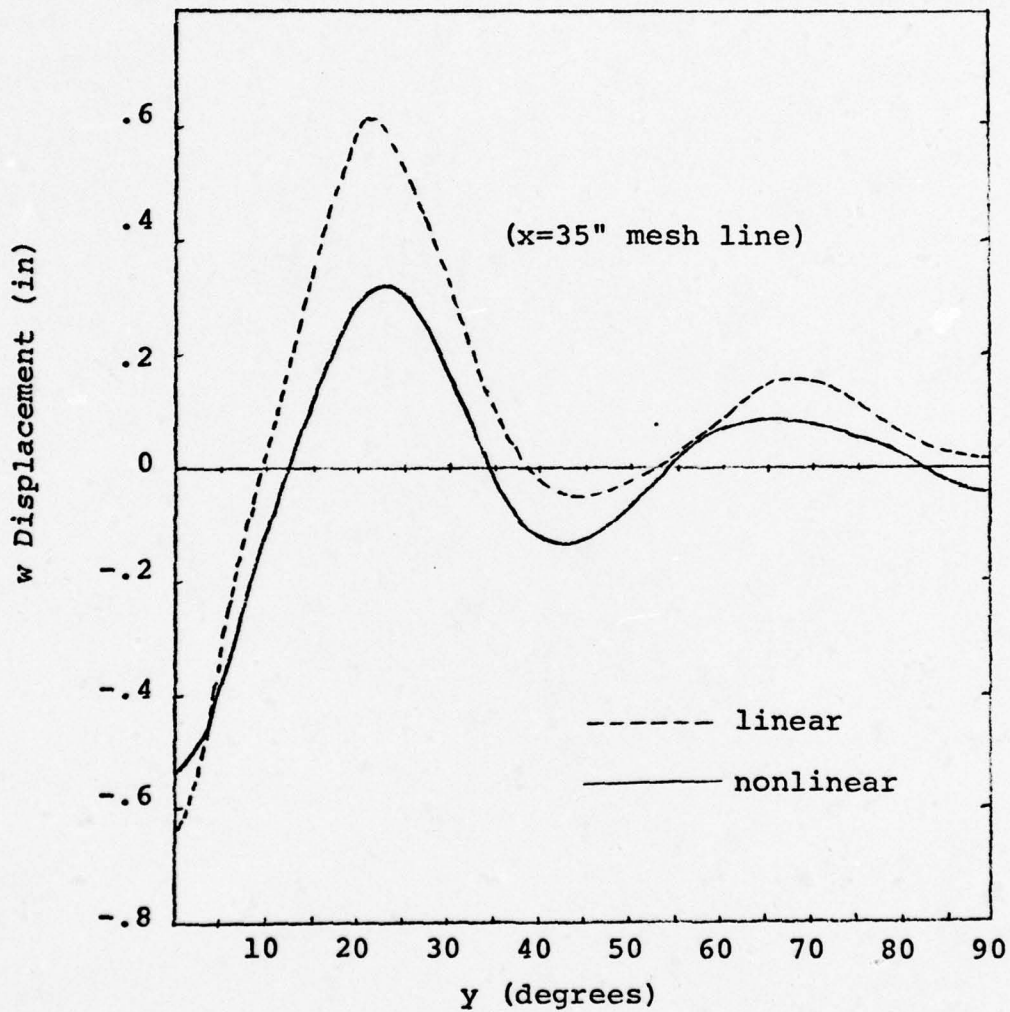


Figure 18. w Displacement Fields Around
24" x 24" Cutout; $t = .2$

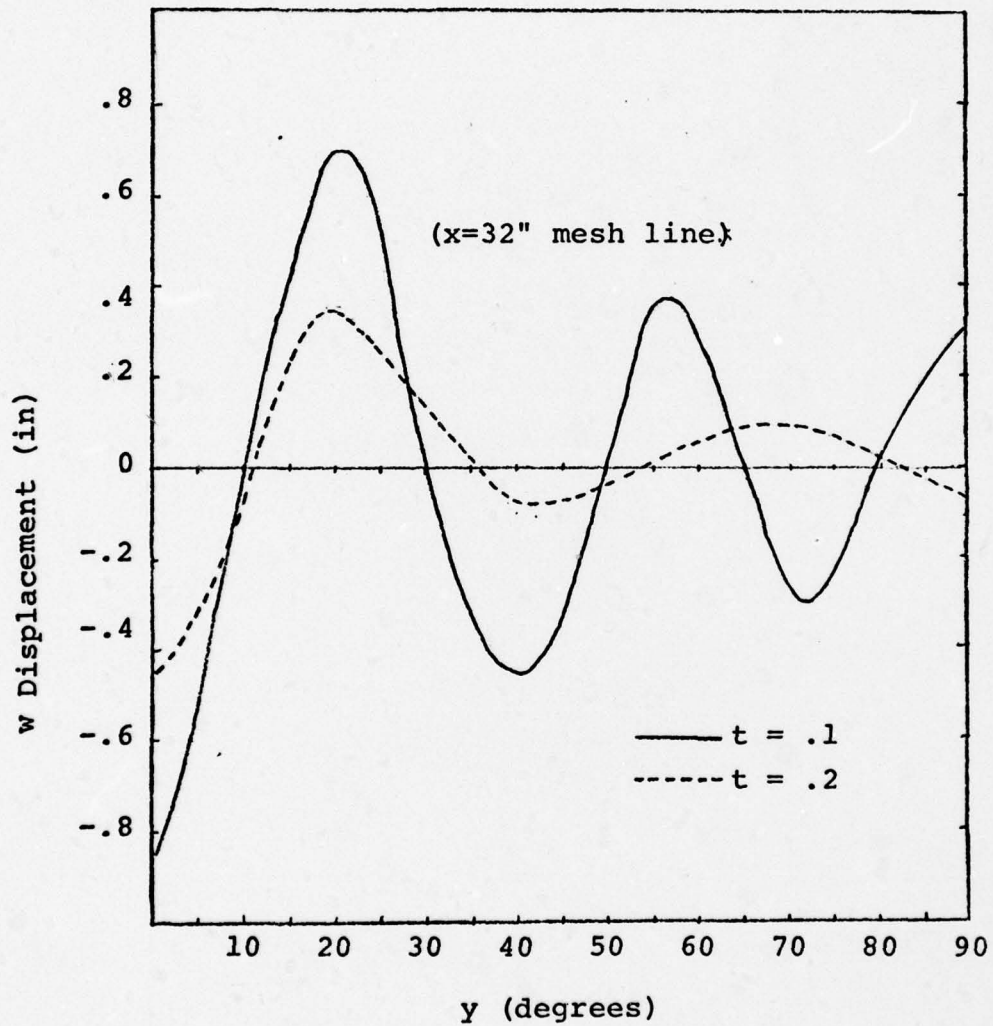


Figure 19. Comparison of Nonlinear Displacement Fields for 24" x 24" Cutouts at Common Loads

TABLE I.

COMPARISON OF LINEAR AND NONLINEAR
RESULTS FOR VARIOUS CUTOUT SIZES

Cutout Size/ Thickness	Linear Bifurcation Pcr	Nonlinear Pcoll
6" x 6" t = .1"	792,100 [#]	No Data
12" x 12" t = .1"	765,780 [#]	655,600 [#]
24" x 24" t = .1"	646,900	608,600 [#]
24" x 24" t = .2"	1,496,000 [#]	1,750,000 [#]

quite close. One thing that must be mentioned is that a stiffened shell analyzed under the usual analytical techniques will not allow the stiffener to resist a rotation directly along its centroidal axis, other than a shear moment. For example, a stringer running in the axial direction cannot resist a circumferential moment. This precludes any assistance that the stiffener may possibly give to the shell in the circumferential direction. It is the authors belief that the collapse load for the shell containing the 12 x 12 cutout, using a nonlinear analysis, would be closer to the critical load obtained from a linear analysis if this previously discussed limitation was eliminated. To improve upon this limitation would require that the stiffener be considered a two dimensional plate structure branching out from the skin surface. The version of STAGS presently used in this thesis did not include this capability. This observation has been varified in a bending study discussed subsequently in this thesis.

IV. Plasticity Analysis of Axially Loaded Cylinder

Description of Model

The cylindrical model used for this study was structured to investigate the effects of material nonlinearity on collapse. Table I presents the stress-strain data in tabular form. Figure 20 depicts the actual stress strain curve for the material, 304 Stainless Steel. The basic shell parameters are

$$\frac{L}{r} = 25$$

$$\frac{r}{t} = 50$$

A length to radius ratio of 25 puts this shell in the general category of long shells. Shells lying in the region of $10 \leq \frac{L}{r} \leq 15$ are usually classified as being of intermediate length. To be classified as short a $\frac{L}{r}$ ratio of less than 10 is considered rule of thumb.

A radius to thickness ratio of 50 is considered quite thick. This condition was desired to better illustrate the effects of plastic deformation. In many aerospace applications thin shells with a r/t of 400 are quite common.

The variable mesh network is presented in Figure 21. A preponderance of nodes are located in the region of greatest displacement gradients.

Again, only one quarter of the shell need be analyzed due to a plane of symmetry normal to the cylinder axis at midlength and an axial plane of symmetry along the cylinder.

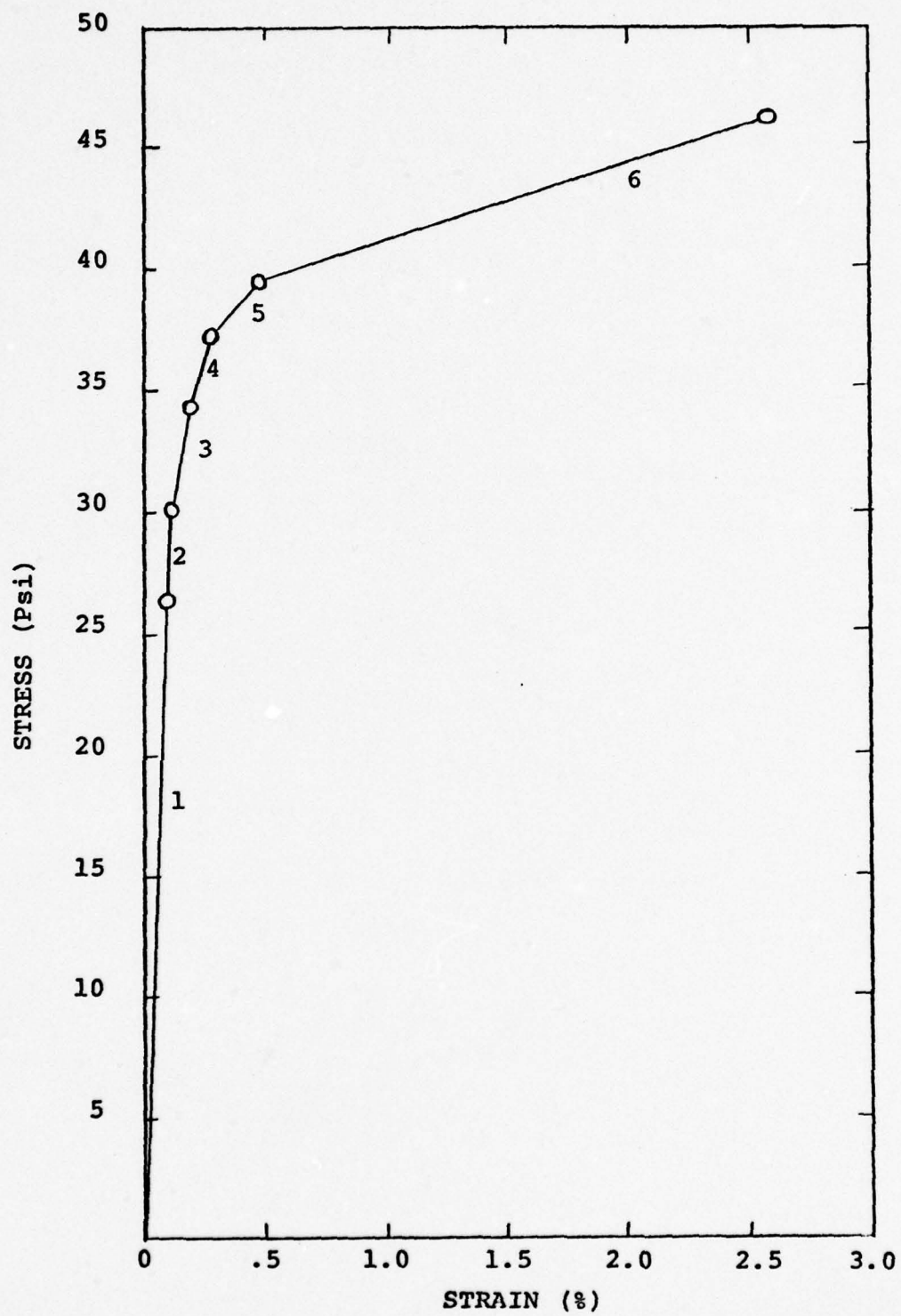


Figure 20. Stress-Strain Curve

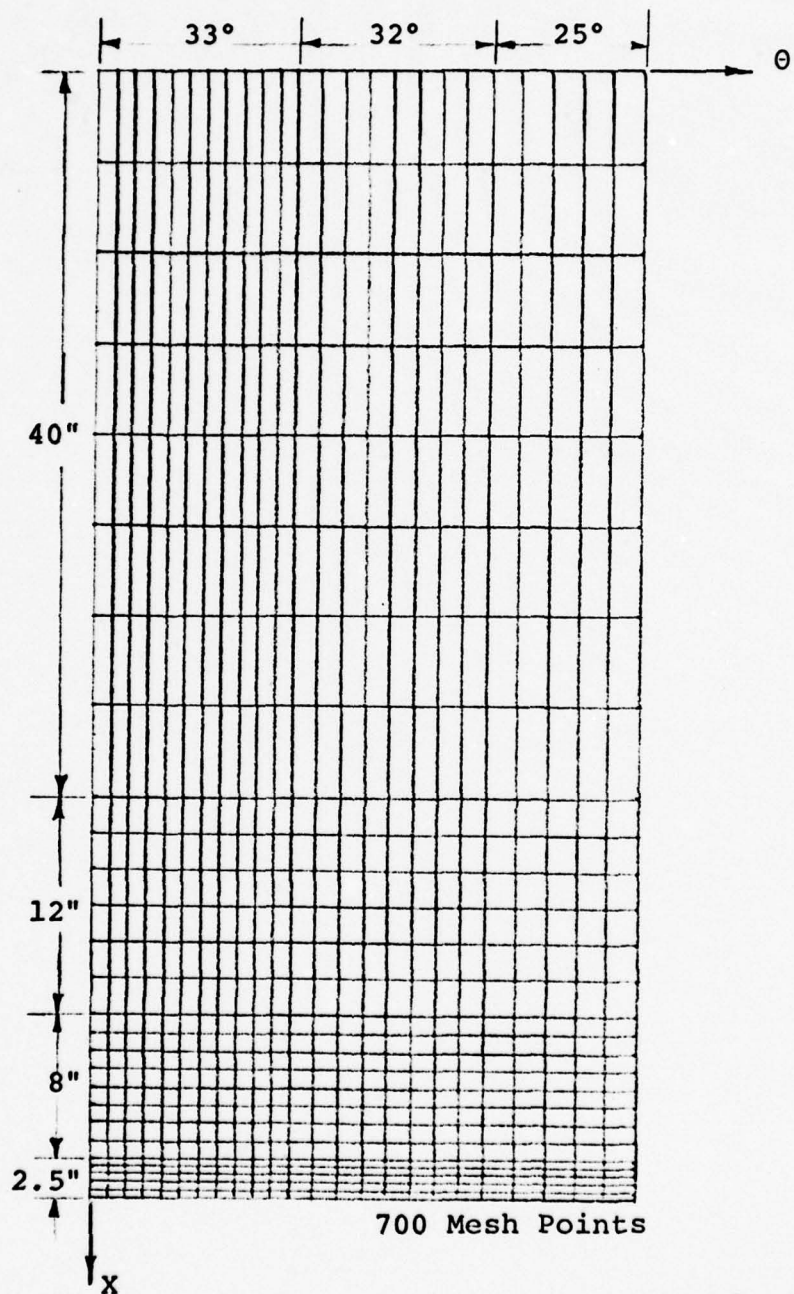


Figure 21. Finite Difference Mesh for
Axial Loaded Cylinder - No Cutout

The boundary conditions imposed upon the shell are depicted in Figure 22. Boundary lines 2, 3, and 4 have symmetric boundary conditions. These edge conditions are interpreted in terms of the w , v , u , and β displacements where w , v , and u are displacements in the direction of the coordinates z , y , and x , respectively, and β is the rotation around a tangent to the edge. Symmetric boundary conditions, as before, imply that

$$u = \beta = 0 \quad \text{On line 3}$$

$$v = \beta = 0 \quad \text{On lines 2 and 4}$$

Boundary line 1 allows freedom of movement in the v and u directions while forcing no movement in the w , v , and β directions. A cylinder under this set of boundary conditions is referred to as being clamped.

The cylinder described above was modeled with an identical stress strain curve as the cylinder under pure bending (See Figure 20). Thus, the parameters defining plastic deformation are identical for both of cylinders lacking cutouts in this thesis.

Results

For inelastic stability Gera d (Ref 13) derived the following plasticity reduction factor for moderate length cylindrical shells under axial compression:

$$\eta_s = \left(1 - \frac{vE}{p} \frac{2}{2}\right)^{3/4} \left(\frac{E_s}{E}\right)^{1/2} \quad (22)$$

For the cylindrical shell model discussed in this study the following constants apply:

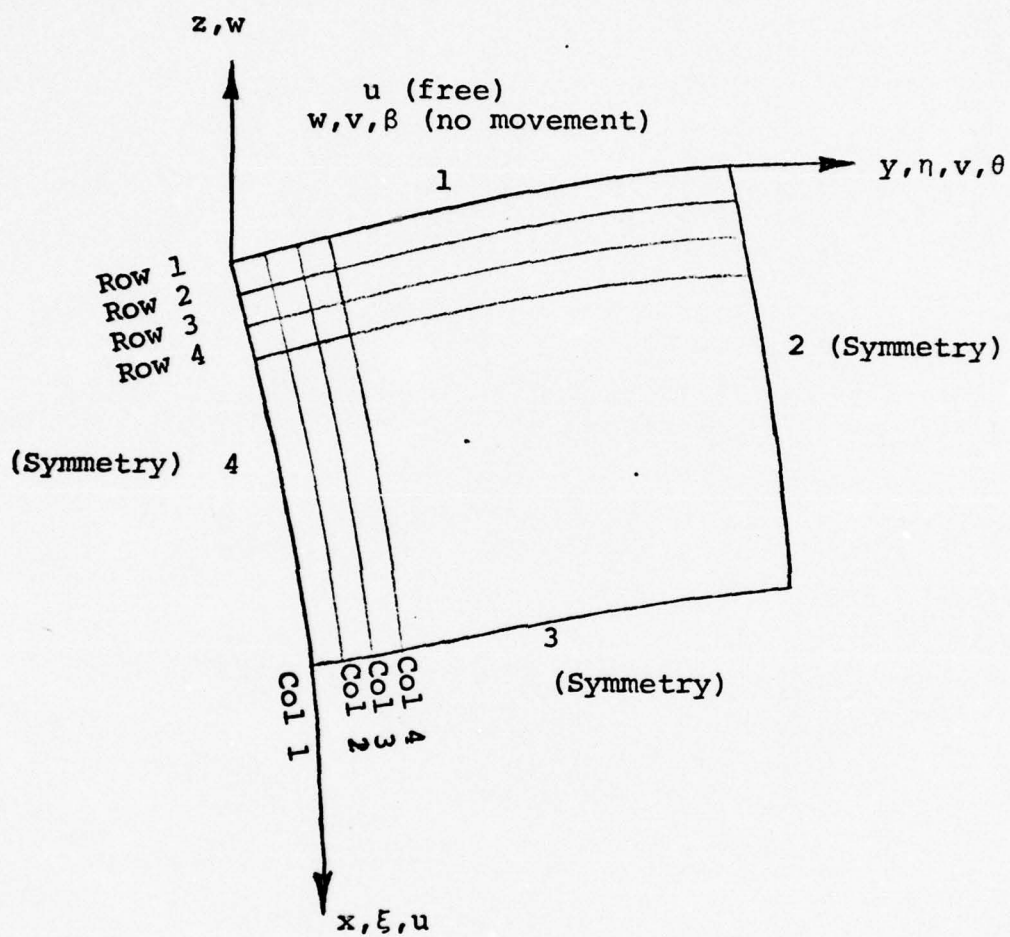


Figure 22. Boundary Conditions for Axially Loaded Cylinders

$$\nu_E = 0.333$$

$$\nu_P = 0.4$$

$$E_S = 50 \times 10^4 \text{ psi}$$

$$E_P = 28.3 \times 10^6 \text{ psi}$$

Substituting these constants into Eq (22) results in a plasticity reduction factor of 0.139. Thus, Gerard's results tells us to expect the plastic collapse load, P_{coll} , to be 13.9% of the linear result. A bifurcation analysis of the shell results in a critical load of 806.5 kips. The nonlinear plastic analysis carried out on the same shell indicates a collapse load of 99.8 kips. (Figure 23) This is a knockdown factor of .124, surprisingly close to that predicted by Gerard.

To shed light on the mechanisms involved in such a drastic reduction in load carrying capability, the stress field around the midsection of the shell was studied for both the linear elastic and plastic analyses.

As seen in Figure 24 the stress field in the circumferential direction is remarkably different for the two analyses. The nonlinear, plastic analysis reveals a smooth sinusoidal transition, for the outer surface, from a positive stress to a negative one of equal magnitude. The reverse is true for the inner surface. Thus, exactly one half of the shell midsection is experiencing a compressive stress, the other half a tensile load. This phenomenon indicates an almost pure

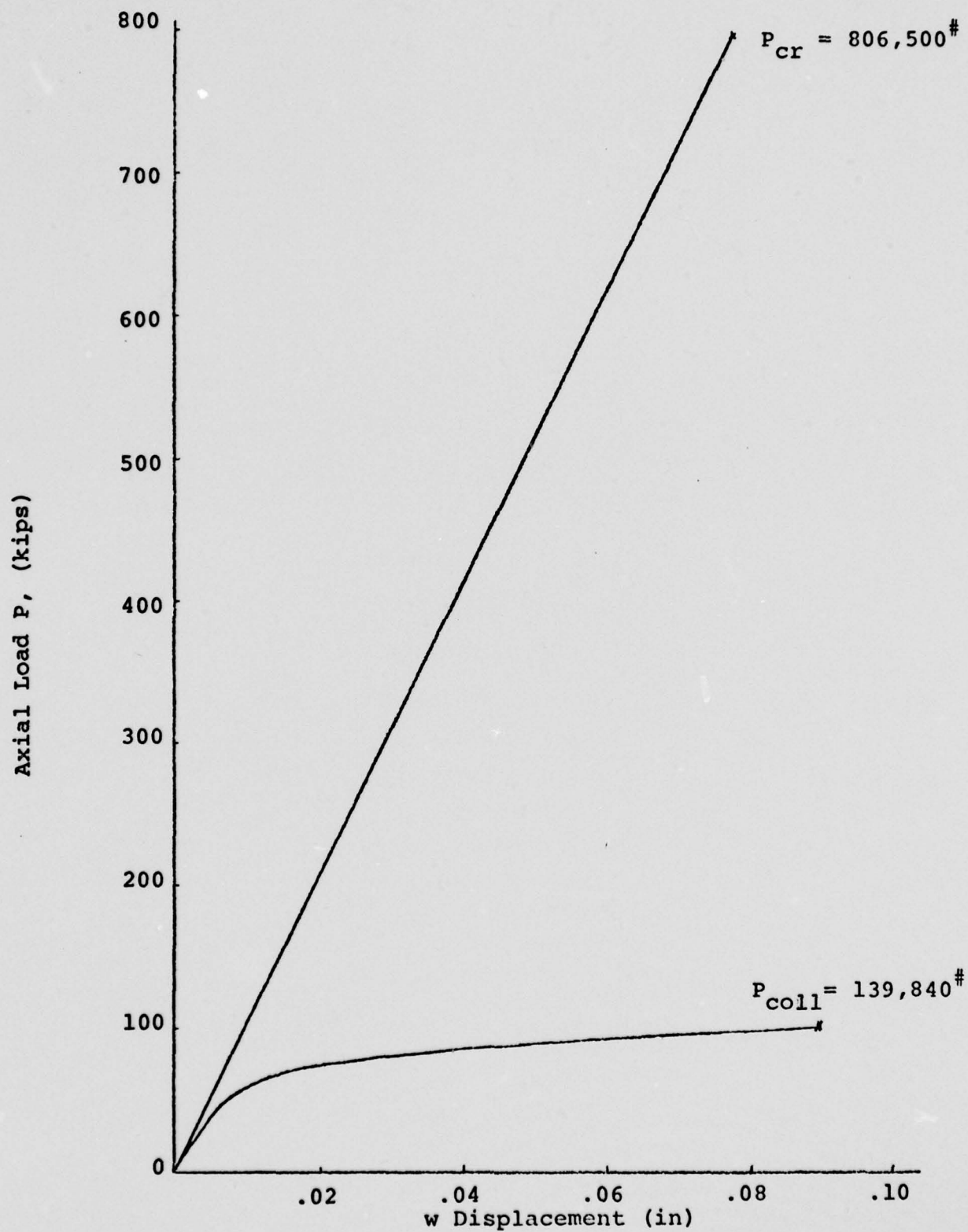


Figure 23. Load-Deflection Curve for Plastic Analysis

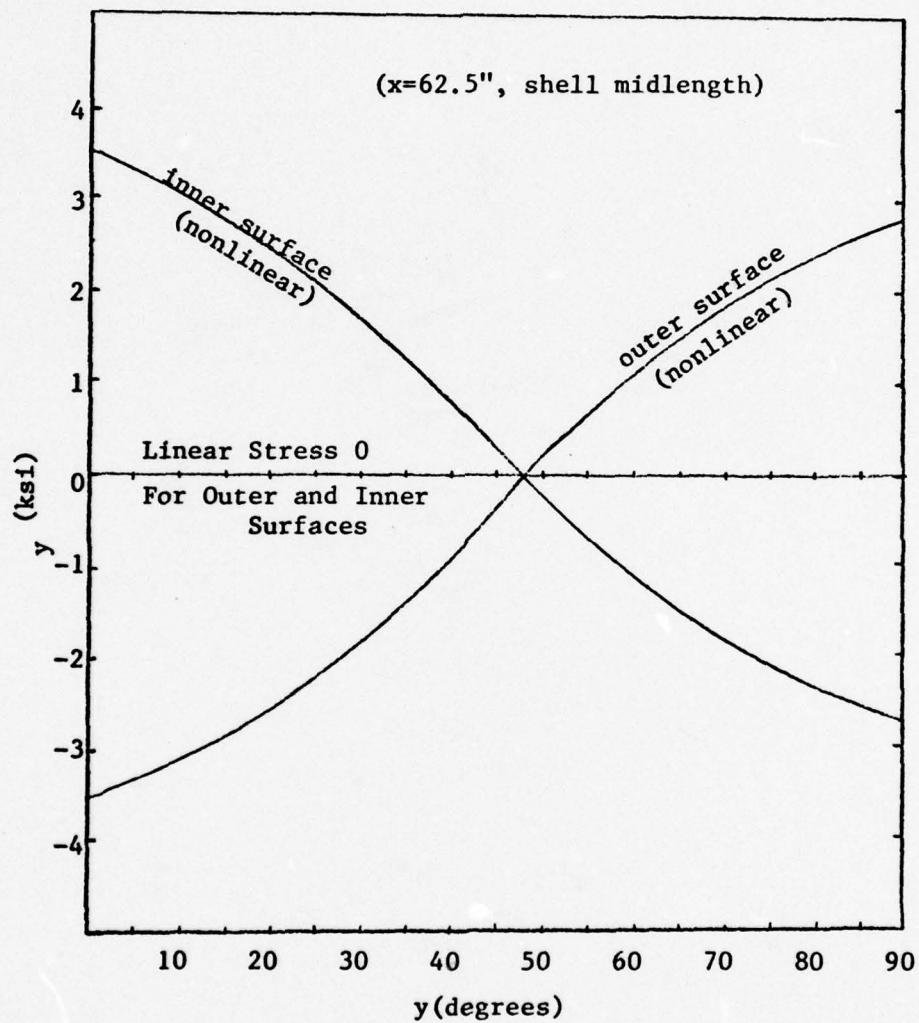


Figure 24. Stress Field in Circumferential Direction for Plastic and Linear Analysis

bending load at the shell midsection with the shell membrane stress being very close to zero.

In the linear analysis the stresses are not large on the outer and inner surfaces of the shell midsection. This indicates a substantially lower moment field existing in the area.

Displacement curves (Figure 25) bear this out. The plastic displacements at the shell midsection are very much larger than the corresponding linear displacements. In this case plasticity is acting very much like a cutout. It is allowing a larger displacement field to occur, making the effect of stress resultants more pronounced. Figure 26 reveals that the linear and nonlinear stress resultant fields are very close. This suggests that the larger displacement field generated by a plastic analysis is making the shell much weaker than the same shell with a smaller displacement field subjected to the same stress resultants. It is this highly nonlinear coupling effect between displacement, moment, and stress resultants that lead to collapse of the shell in a plasticity analysis.

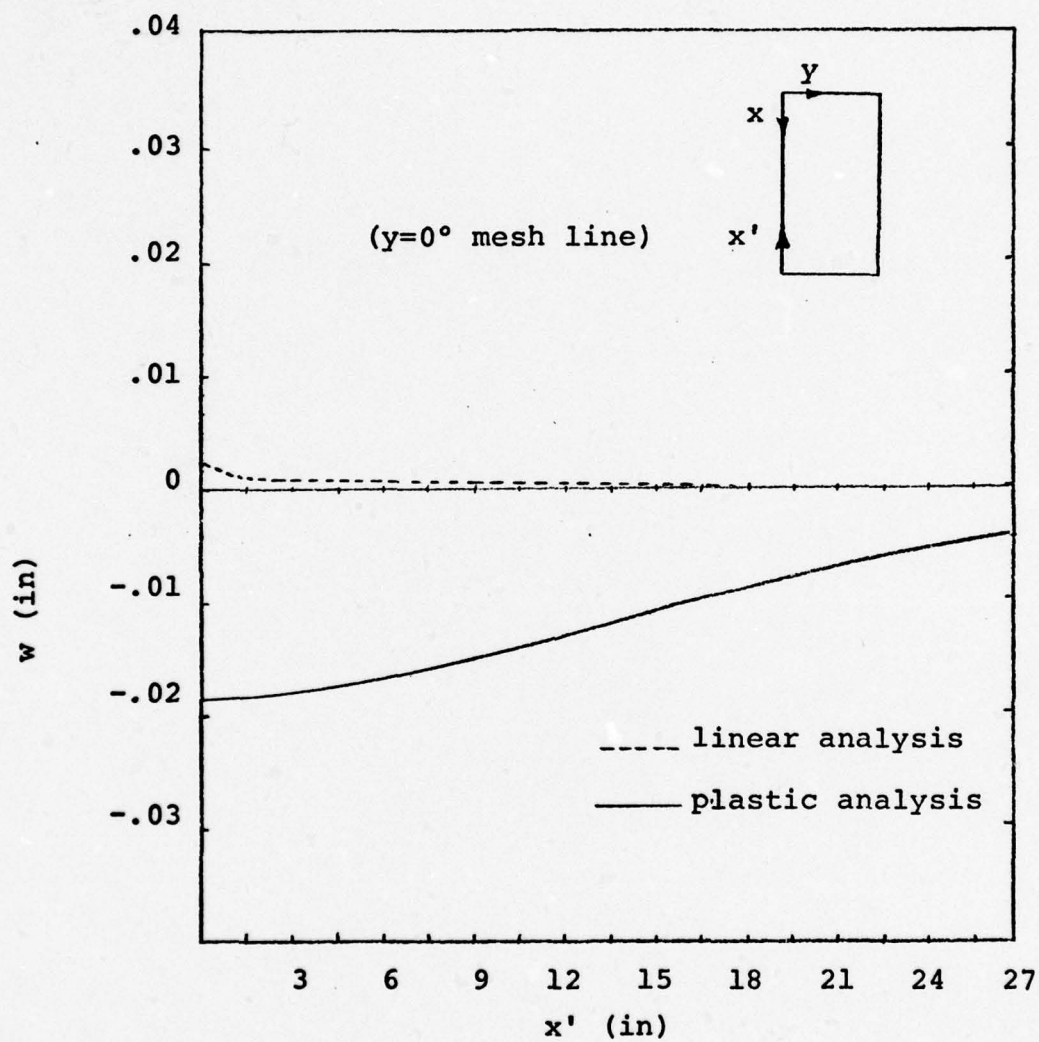


Figure 25. Displacement Curves for Plastic and Linear Analysis

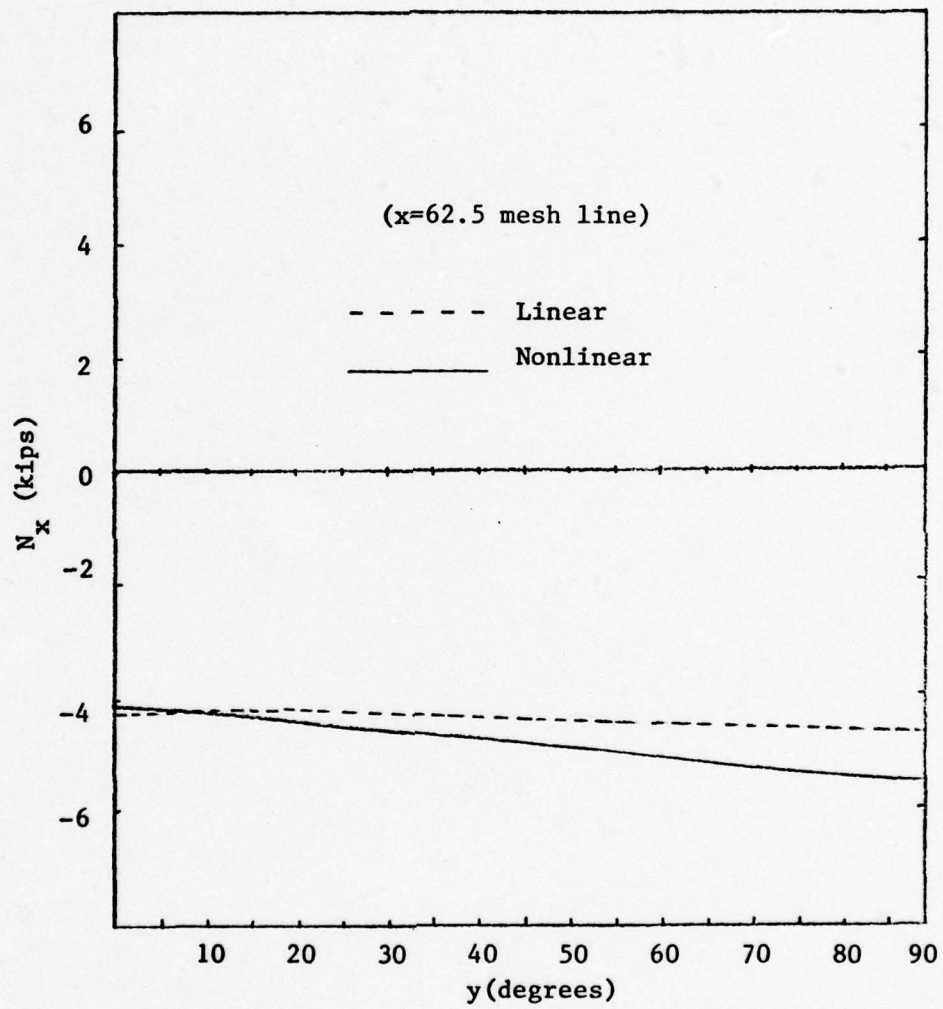


Figure 26. Linear and Nonlinear (Plastic) Stress Resultants

V. Cylindrical Shell Under a Pure Bending Load

Description of the Model

The major thrust of this particular study was directed at the effects of boundary conditions and end-ring stiffening on a cylinder loaded in bending. The cylindrical model chosen for this case was an isotropic cylinder (no cutout) with the following geometric and material properties:

$$\frac{r}{t} = 50$$

$$E = 28.3 \times 10^6 \text{ psi}$$

$$\nu = .3$$

$$\frac{L}{R} = 25$$

The material is 304 Stainless Steel with a yield stress of 37,700 psi. The stress strain curve is shown in Figure 20. The piecewise linear representation of the stress-strain curve for 304SS at room temperature is listed in Table II.

The loading and shell geometry are shown in Figure 27. The end load N_x applied to generate the required bending moment takes the form

$$N_x = -N \cos \theta \quad (25)$$

where N is the amplitude of the load and θ being the circumferential coordinate. The bending moment generated is

$$M = N\pi r^2 \quad (26)$$

This study required that only one-quarter of the shell be analyzed due to a plane of symmetry normal to the cylinder axis at midlength and an axial plane of symmetry passing through points of maximum bending load. Symmetry conditions

Table II.

PIECEWISE LINEAR REPRESENTATION OF STRESS-STRAIN
CURVE FOR 304SS @ ROOM TEMPERATURE

SEGMENT	σ_{Begin} (PSI)	σ_{End} (PSI)	ϵ_{Begin}	ϵ_{End}
1	0	26250	0	.00095
2	26250	3000	.00095	.00125
3	30000	34250	.00125	.00200
4	34250	37250	.00200	.00300
5	37250	39500	.00300	.00500
6	39500	46250	.00500	.02625
7	46250	100,000	.02625	0.200

are applied at the three boundaries designated in Figure 27. The fourth boundary is restrained by two stiffening end rings. The rings are used to provide as much of an undistorted cross-section as possible. The rings possess enough of a stiffening effect to approximate a condition in which the end plane rotates and translates with a minimum of cross-sectional warping.

It is extremely important in this study that the end-plane of the shell be free from warping. Any significant deviation from a warp free end plane results in a load that is not pure bending.

Both single ring and double ring stiffeners were investigated until it was evident that two rings were significantly better suited to prevent undesirable warping. In all, seven cases were analyzed; Figure 28 depicts a profile of the cross sectional warping for three of these cases. In the model the end rings are located at X equal to 0, and 0.02L. The rings that provided the best warping characteristics possess the following non-dimensional parameters:

$$\begin{aligned}\frac{A}{r^2} &= .02 \\ \frac{I}{r^4} &= 1.6\end{aligned}\tag{27}$$

where I is the cross-sectional moment of inertia about the centroidal axis normal to the plane of the ring and A is the cross-sectional area of the ring. The torsional stiffness of the rings as well as the other stiffnesses, were considered to be zero. The rigid body displacement of the cylinder

Restraining
Point
($w=0$)

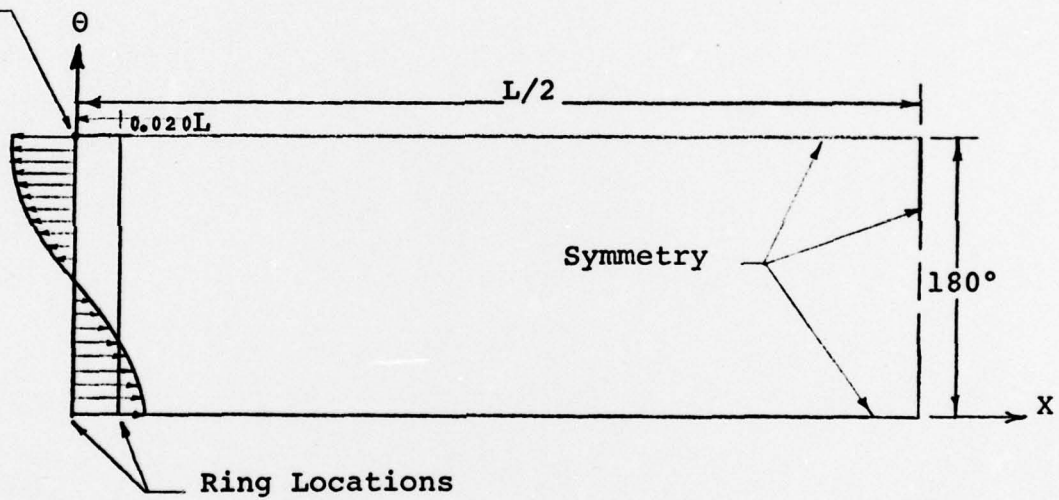


Figure 27. Analytical Model

was prevented by specifying that the lateral displacement was zero at $w(0,180^\circ)$ (See Fig 27).

The grid spacing for this model was varied in both the axial and circumferential directions providing a 50 by 21 point grid network. The variable spacing is included to allow a higher concentration of grid points in areas where failure is expected to occur. In the axial direction failure is expected at the cylinder midlength so mesh density is increased near that locale. (See Figure 29)

Additional Comments on Ring Stiffener Configuration and Boundary Conditions

For stiffened shells under bending or axial loads, rotational restraint is a major factor in buckling. It was found in this study that warping could not be prevented by the use of just one stiffening ring, even if that ring possessed very large moments of inertia. It was discovered that by placing two rings a distance $0.02L$ apart, a couple was generated when the structure was loaded that counteracted the moments trying to warp the end plane. This double ring stiffening effect is necessary in much the same manner that the stiffening plate is needed to generate rotational rigidity for the axially compressed, stringer stiffened shells discussed earlier in this thesis.

The boundary conditions also play a major role in the warping problem. By allowing β to be free the shell, by itself, lacks the required rigidity to prevent warping. Only by the introduction to two rings into the analysis is the required rigidity obtained.

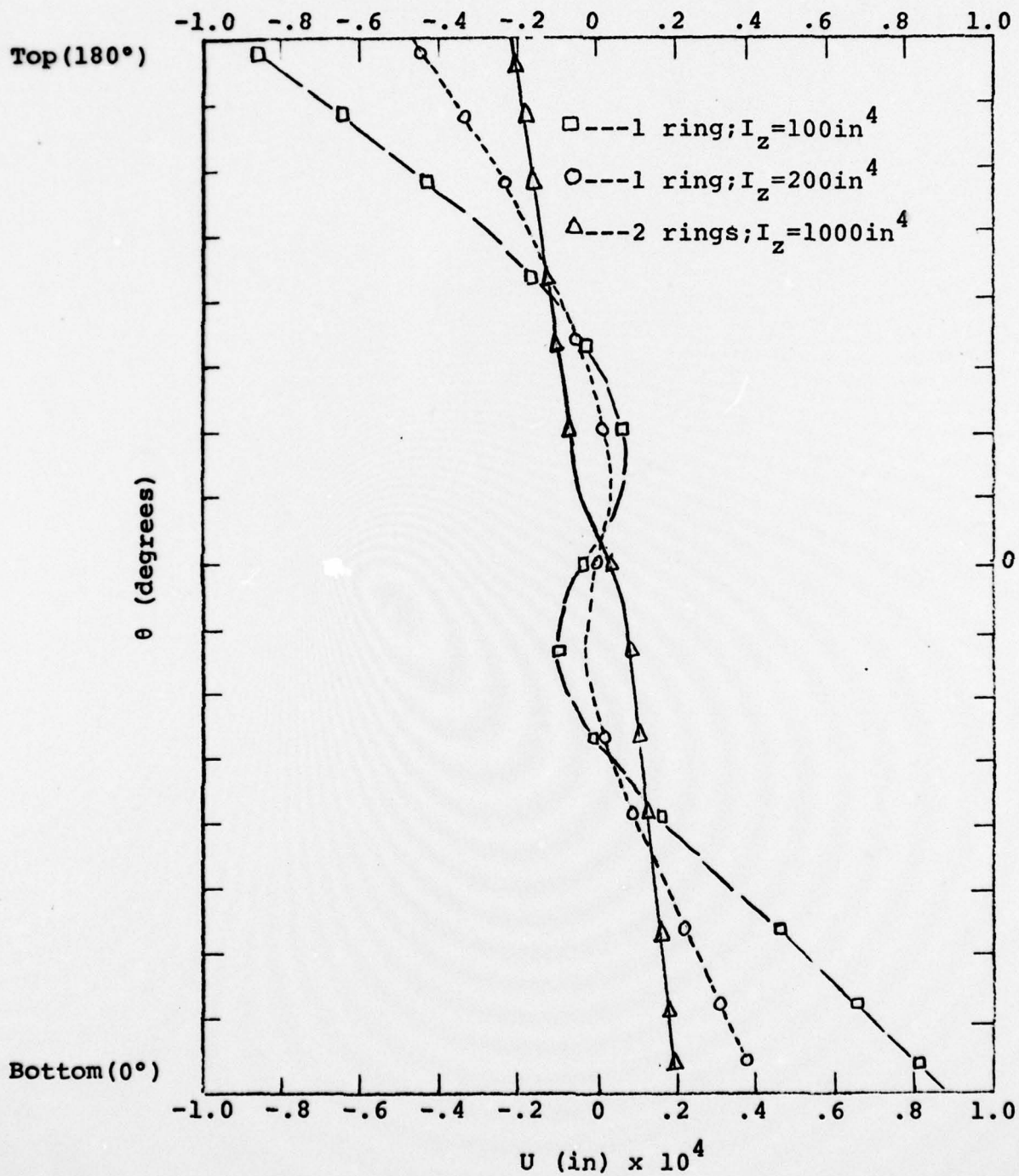


Figure 28. Warping Plane Profiles for Various Ring Stiffness Configurations

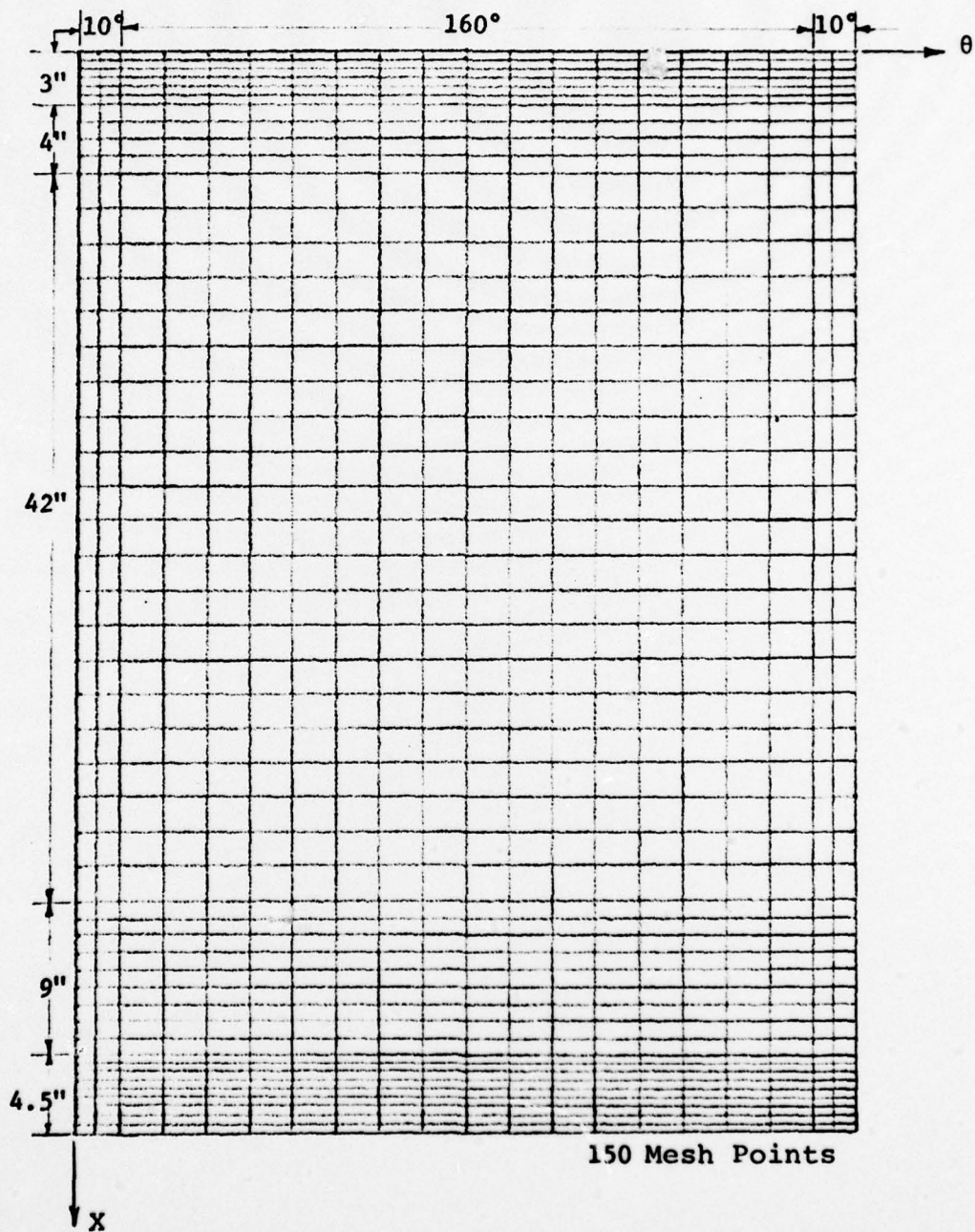


Figure 29. Finite Difference Mesh for
End Moment Loading Case
No Cutout

VI. CONCLUSIONS

The following conclusions can be made.

- (1) The bending moment in a nonlinear analysis has a great effect on a flexible shell structure, less effect on a less flexible one. This particular characteristic is not present in a linear analysis due to the removal of the higher order rotation terms that effect strain.
- (2) It is necessary to allow stiffeners to resist rotations directly along their centroidal axes, caused by moments along this axis, so that rings or stringers are able to assist the shell membrane in resisting rotations.
- (3) In order for this rotational rigidity to be effectively displayed by stiffeners, the stiffener itself must be considered a two-dimensional plate structure branching out from the shell skin. The usual techniques published in the technical literature normally handles the analysis of stiffeners as if they were beams. Consequently, their true rotational effect (as required by conclusion #2) is not analytically displayed.
- (4) Displacement fields are the primary source of comparison in evaluating the shell load carrying capability because they best reflect the stiffness of the shell
- (5) It becomes clear through this study that cutouts positioned within cylindrical shells create results that are not easily predictable using past shell

experiences. This idea should be tied in very closely with the analytic inaccuracies associated with the analysis of the stiffening of the shell. (Refer to Conclusion #2).

- (6) As the shell thickness becomes larger the nonlinear collapse analysis gives results that indicate a greater rigidity than one could conclude from a linear bifurcation analysis.
- (7) An elastic/plastic analysis appears to precipitate collapse in much the same manner as do cutouts.
- (8) The collapse results obtained using both geometric and material nonlinearities as incorporated into the STAGS plasticity subroutine can be closely approximated using Gerard's plasticity equation.
- (9) The White-Besseling technique of plastic analysis for a shell under compression gives reasonable results. It is required that a great deal of computer time is consumed for a complete solution. Therefore, this author recommends that an approximate analytical calculation be carried out first so that the analyst obtains an approximate idea of the computer time necessary before attempting a lengthy computer solution.
- (10) In order to apply an analogous pure bending load at the extreme ends of a cylindrical shell, one must prevent warping of the end cross sections.
- (11) The boundary conditions associated with proper warping constraints as pertaining to the previous conclusion should be:
v, β directions - no movement
w, u directions - movement
at boundary line 1.

(12) With β being fixed it is required that the analyst recognize that the shell, by itself, cannot establish the required rigidity. Consequently, to associate this boundary with the zero warping requirement, one must fix to the end of the shell ring stiffeners. In order to conform to conclusion #2 it is required that two rings, separated by a given distance, be placed into the analysis. This distance of separation is specified by the parallel axis for moment of inertia.

Bibliography

1. Hoff, N.J. "The Perplexing Behavior of Thin Cylindrical Shells Under Axial Compression". Israel J. Technol, Vol 4, pp. 1-28, 1966.
2. Timoshenko, S.P., and Gere, J.M. Theory of Elastic Stability (Second Edition). New York: McGraw-Hill Book Co., Inc., 1961.
3. Seide, P., and Weingarten, V.I. "On the Buckling of Circular Cylindrical Shells Under Pure Bending." Journal of Applied Mechanics, 28: 112-116, (1961).
4. Palazotto, A.N. "Bifurcation and Collapse Analysis of Stringer and Ring Stringer Stiffened Cylindrical Shells with Cutouts." Computers and Structures, Vol. 7, pp. 47-58, (1977).
5. Brazier, L.G. "On the Flexure of Thin Cylindrical Shells and Other Thin Sections." Proceedings of the Royal Society, Series A, 116: 104-114, (1926).
6. Aksel'rad, E.L., "Refinement of the Upper Critical Loading of Pipe Bending Taking Account of the Geometrical Nonlinearity." AIAA Journal, 2: 1437-1440, (1964).
7. Sobel, L.H., "On the Buckling of Cylindrical Shells Under Pure Bending." U.S. Atomic Energy Commission, E(11-1)-3045, November, 1975.
8. Brogan, F. and Almroth, B., "Buckling of Cylinders with Cutouts." AIAA Journal, 8: 236-240, February, 1970.
9. Sobel, L.H., and Newman, S.Z., "Instability Analysis of Elbows in the Plastic Range." Westinghouse Advanced Reactors Division, E(11-1)-3045, November, 1976.
10. Stevens, W.B., and J.H. Starnes, and B.O. Almroth. "Collapse of Long Cylindrical Shells Under Combined Bending and Pressure Loads." AIAA Journal, 13:20-25, January, 1975.
11. Almroth, B.O., F.A. Brogan, F. Zele. "User's Manual For the STAGS-A Computer Code." Collapse Analysis for Shells of General Shape, Vol. II, AFFDL-TR-71-8, March 1973.

12. Sobel, L.H. "On the Basic Concepts of the Instability of Structures." U.S. Atomic Energy Commission, E(11-1)-3045, November, 1975.
13. Gerard, G. Introduction to Structural Stability Theory. New York: McGraw-Hill Book Co., Inc, 1962

VITA

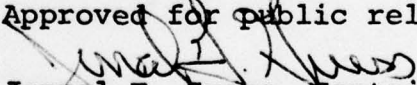
Norton Leslie Compton was born on 21 October 1954. He graduated from Valley High School in Las Vegas, Nevada in 1972 and attended Virginia Tech from which he received the degree of Bachelor of Aerospace and Ocean Engineering in June 1976. Upon graduation, he received a commission in the United States Air Force through the ROTC program. Upon entering active duty in August 1976 he was assigned to the School of Engineering, Air Force Institute of Technology. His next assignment is to the Space and Missile System Organization under the Directorate for Advanced Space Programs.

Permanent Address:

122 Country Club Drive
Williamsburg, VA 23185

UNCLASSIFIED

SECURITY CLASSIFICATION OF THIS PAGE (When Data Entered)

REPORT DOCUMENTATION PAGE		READ INSTRUCTIONS BEFORE COMPLETING FORM
1. REPORT NUMBER AFIT/GA/AA/77D-2	2. GOVT ACCESSION NO.	3. RECIPIENT'S CATALOG NUMBER
4. TITLE (and Subtitle) NONLINEAR COLLAPSE ANALYSIS OF CYLINDRICAL SHELLS		5. TYPE OF REPORT & PERIOD COVERED MS Thesis Jan 77 - Dec 77
		6. PERFORMING ORG. REPORT NUMBER
7. AUTHOR(s) Norton L. Compton 2/Lt USAF		8. CONTRACT OR GRANT NUMBER(s)
9. PERFORMING ORGANIZATION NAME AND ADDRESS Air Force Institute of Technology (AFIT/EN) Wright-Patterson AFB, OH 45433		10. PROGRAM ELEMENT, PROJECT, TASK AREA & WORK UNIT NUMBERS
11. CONTROLLING OFFICE NAME AND ADDRESS		12. REPORT DATE 9 December 1977
		13. NUMBER OF PAGES 78
14. MONITORING AGENCY NAME & ADDRESS (if different from Controlling Office)		15. SECURITY CLASS. (of this report) Unclassified
		15a. DECLASSIFICATION/DOWNGRADING SCHEDULE
16. DISTRIBUTION STATEMENT (of this Report) Approved for public release; distribution unlimited.		
17. DISTRIBUTION STATEMENT (of the abstract entered in Block 20, if different from Report)		
18. SUPPLEMENTARY NOTES Approved for public release; IAW AFR 190-17  Jerral F. Guess, Captain, USAF Director of Information		
19. KEY WORDS (Continue on reverse side if necessary and identify by block number) Cylindrical Shells Stiffened Shells Shells with Cutouts		
20. ABSTRACT (Continue on reverse side if necessary and identify by block number) This study was carried out to determine the effects of plasticity and cutouts on the buckling of stiffened and nonstiffened cylindrical shells. Axial and end moment loading configurations were considered. The problem was investigated using the nonlinear and linear branches of the STAGS (Structural Analysis of General Shells) computer code. It becomes clear through this study that cutouts positioned		

DD FORM 1 JAN 73 1473

EDITION OF 1 NOV 65 IS OBSOLETE

UNCLASSIFIED

SECURITY CLASSIFICATION OF THIS PAGE (When Data Entered)

UNCLASSIFIED

SECURITY CLASSIFICATION OF THIS PAGE(When Data Entered)

↓
within cylindrical shells create results that are not easily predictable using past shell experiences. The moment field in a nonlinear analysis has a much greater effect on a more flexible structure than a less flexible one. This characteristic is not present in a linear analysis due to the removal of the higher order rotation terms that effect strain.

An elastic/plastic analysis appears to precipitate collapse in much the same manner as do cutouts. The collapse results obtained using a completely nonlinear plastic analysis can be closely approximated using Gerard's plasticity equation.

To prevent warping of the end plane under bending two rings separated by a distance d determined by the parallel axis theorem are needed to counteract the lack of rotational rigidity in the shell.

UNCLASSIFIED

SECURITY CLASSIFICATION OF THIS PAGE(When Data Entered)